Metamorphic evolution of the Gran Paradiso Massif: A case study of an eclogitic metagabbro and a polymetamorphic glaucophane-garnet micaschist.

Metamorphic evolution of the Gran Paradiso Massif: a case study of an eclogitic metagabbro and a polymetamorphic glaucophane-garnet micaschist

Ivano Gasco[1,*], Alessandro Borghi [2] and Marco Gattiglio[1]

[1] Università degli Studi di Torino, Dipartimento di Scienze della Terra, Via Valperga Caluso 35, I-10125 Torino, Italy

[2] Università degli Studi di Torino, Dipartimento di Scienze Mineralogiche e Petrologiche, Via Valperga Caluso 35, I-10125 Torino, Italy

[*] Tel: +39 0116705335; Fax: +39 0116705339; E-mail: ivano.gasco@unito.it

Abstract. Sub-continental type gabbro preserving an eclogite facies assemblage and glaucophane-garnet bearing micaschist from the eastern border of the Gran Paradiso Massif (Western Alps) have been investigated to constrain its tectono-metamorphic evolution. Glaucophane-bearing metapelites were never reported before while metagabbros are only found in the southern part of the Massif. Growth zoning of multistage garnet in metapelites and the investigation of two different chemical systems (metapelitic and basic), allowed to reconstruct the PT path followed by Gran Paradiso Massif during the late Variscan stage and during the Alpine orogeny. Micro-structural investigations allowed to identify different assemblages related to different tectono-metamorphic stages. Pseudosection modelling with the software PERPLE_X of the stable assemblages and of the mineral compositions has allowed to infer the PT conditions for these different metamorphic stages. Variscan metamorphism reached 620-630 °C at 8-9 kbar. The Alpine HP stage peaked at 580-600°C and 26-27 kbar and the first decompression stage was at 580-610°C and 21-22 kbar with no T increase before the development of the S_1 regional foliation. S_1 represents the main tectono-

metamorphic event recorded by Gran Paradiso Massif and developed at 600-625 °C and 9.5-11.5 kbar in the low T and high P amphibolite facies. From these data a different PT path is proposed respect to previous works. The exhumation from peak eclogite facies conditions to amphibolite facies was nearly isothermal and then was followed by considerable cooling suggesting a two-stage exhumation process controlled by different mechanisms.

Key-words: Gran Paradiso, polycyclic metamorphism, PT path, exhumation, pseudosection, Western Italian Alps.

1. Introduction

Reconstruction of PT paths by means of the analysis of phase equilibria in metamorphic rocks is an essential tool in constraining models of the tectonic evolution of mountain belts. The Western Alps offer an excellent opportunity for studying the metamorphic and tectonic processes developed during subduction as well as the exhumation of deep-seated rocks.

High-pressure relics in the continental basement of the Gran Paradiso Massif are represented by different rock-types such as fine-grained eclogites, eclogitic metagabbros, whiteschists and garnet-chloritoid bearing micaschists (Compagnoni & Lombardo, 1974; Dal Piaz & Lombardo, 1986; Biino & Pognante, 1989; Le Bayon & Ballèvre, 2006; Gabudianu Radulescu et al., 2009). Biino & Pognante (1989) reported for the first time continental-type gabbros within a Variscan basement in the Internal Crystalline Massifs. These late-Paleozoic gabbros outcrop in the southern part of the Gran Paradiso Massif, in the Vallone di Sea, and show a static eclogite facies metamorphism followed by dynamic recrystallization under blueschist facies conditions. They estimated peak conditions around 18-20 kbar at 500-550°C using classical geotermobarometry. Eclogitic metagabbros associated to glaucophane-garnet bearing micaschists have been also reported by Gasco et al. (2009) at the eastern border of Gran Paradiso basement.

In this study, the pseudosection approach (Connolly, 1990) was applied to metabasic and metapelitic rocks outcropping in the eastern side of the Gran Paradiso Massif (Orco Valley, Western Alps) in order to estimate the PT conditions attained during the eclogitic peak metamorphic event and to better constrain the PT path followed during their exhumation.

Two different chemical systems have been investigated: basic (eclogitic metagabbro) and pelitic (glaucophane-bearing micaschist with multistage garnet). These rocks contain well preserved evidence of a sequence of high-pressure stages that allowed to reconstruct the early-Alpine subduction event for the Gran Paradiso Massif. Pseudosection modelling has permitted to reconstruct a portion of the metamorphic PT path followed by the polymetamorphic rocks of the Gran Paradiso Massif on the basis of garnet growth zoning and of chemical composition and micro-structural relationships of the other minerals. Moreover, multistage garnet from the metapelite sample allowed to evaluate the pre-Alpine peak T metamorphism. The inferred PT path has been integrated with the tectonic evolution proposed by Gasco et al. (2009) and with the chronological data available from literature, suggesting a two-stage process for the exhumation of the Gran Paradiso Massif.

2. Geological setting

The Gran Paradiso Massif (Fig. 1) belongs to the Penninic Zone of the Western Italian Alps and together with Monte Rosa and Dora Maira nappes defines the Internal Crystalline Massifs. They are the deepest tectonic elements of the Western Alps and crop out as large axial culminations, overthrusted by different structural elements of the Piedmont Zone. The Gran Paradiso Massif is composed mainly of augen-gneisses (Gneiss Occhiadini Complex) derived from Permian (270 ± 5 Ma) porphyritic granitoids (Bertrand et al., 2000, 2005; Ring et al., 2005), intruded into a metasedimentary high-T Variscan complex (Compagnoni et al., 1974). Well-preserved intrusive contacts are reported at Lake of Teleccio in the Orco Valley (Callegari et al.,

1969; Compagnoni & Prato, 1969) and in Valnontey (Le Bayon & Ballèvre 2006), where relics of the intrusive Variscan structures and sillimanite paragneisses were preserved from Alpine reworking. A monometamorphic complex composed of probably Permo-Carboniferous metasediments known as Money Complex (Compagnoni et al., 1974) and a Permo-Triassic cover comprising quartzites, dolomites and marbles is also present (Elter, 1960; 1971; 1972). At the south-western end of the Massif the cover consists of a Permian metavolcanic and metapelitic sequence, known as Bonneval Unit (Bertrand, 1968). The Variscan metasedimentary rocks were reworked during Alpine orogeny and transformed into a polymetamorphic complex of paragneisses and micaschists (Gneiss Minuti Complex, Compagnoni et al., 1974) with lenses of eclogites interpreted as pre-Alpine amphibolites (Compagnoni & Lombardo, 1974) and Variscan gabbros (Biino & Pognante, 1989). Garnet-omphacite pairs in metabasite were used to estimate minimum PT conditions for the eclogite facies event yielding P > 12–14 kbar and T of 500–550 °C (Brouwer et al., 2002). Higher pressure and similar temperature were inferred by pseudosection modelling of whiteschists (21–23 kbar and 540–570 °C ,Wei & Powell, 2003, 2004; Meffan-Main et al., 2004; 19-27 kbar 515-600 °C, Gabudianu Radulescu et al., 2009). The pseudosection approach also indicated conditions of 18-20 kbar and 480-490 °C for the Gneiss Minuti Complex in the northern part of the Massif (Le Bayon et al., 2006). This high-P event is followed by a late re-equilibration at 4–6 kbar and 500–550 °C interpreted as a re-heating stage occurred after an initial cooling during decompression (Borghi et al., 1996; Brouwer et al., 2002, 2004).

Rb-Sr geochronological data on whiteschists suggest that the eclogite-facies event occurred at 43 ± 0.5 Ma (Meffan-Main et al., 2004) and the greenschist-facies metamorphism at 33-40 Ma (Inger & Ramsbotham, 1997; Freeman et al., 1998; Meffan-Main et al., 2004). In contrast, U-Pb SHRIMP dating on whiteschists allanite yielding 33.7 ± 1.6 Ma is reported by Gabudianu Radulescu et al., (2009) and was interpreted as the age of the HP metamorphic peak. The final stages of exhumation are recorded by U-Pb fission ages on zircon (225 ± 25 °C at 29-33 Ma) and apatite (100 ± 20 °C at 20–24 Ma) (Hurford & Hunziker, 1989, Malusà & Vezzoli, 2006).

2.1 The study area

New detailed mapping at 1:10 000 scale was performed along the eastern border of the Gran Paradiso Massif (Fig. 2) and allowed to reconstruct its structural evolution (Gasco et al., 2009). Eclogite facies assemblages of Alpine age were identified in both the metabasic and the metasedimentary rocks.

The Gneiss Minuti Complex mostly consists of micaschists and minor albite-gneisses with the assemblage Qtz + Wm + Grt + Hbl + Zo/Czo + Ab + Rt (abbreviations of minerals are given according to Kretz, 1983 with the update of Bucher & Frey, 2002), defining the main regional foliation (S_1; Fig. 4a). Rarely, a pre-S_1 foliation is preserved (Fig. 3a, b) and is defined by Qtz + Gln + Wm + Grt + Rt (Fig. 4b, c). Within the metasedimentary complex meso- to macro-scale bodies of metabasites occur. On the basis of structural and metamorphic characteristic two types metabasic rocks have been distinguished:

I. decimetre to metre sized lenses or layers of fine-grained, non-schistose rocks consisting of Grt + Omp + Gln + Wm + Zo + Rt, and
II. decametre to hectometre sized fine- to medium-grained rocks with a well developed foliation defined by Wm + Ca-Am + Zo + Rt ± Chl ± Qtz (Fig. 4d), locally preserving domains with an eclogite facies mineral assemblage of millimetric Omp surrounded by Grt (Fig. 4e).

Type I rocks are interpreted as eclogitized basic dikes, whereas type II as metagabbros with microstructures similar to those already described by Biino & Pognante (1989) in the southern part of the Gran Paradiso Massif. Metagabbroic rocks consist of one metabasic body of 100-150 m thickness with locally well-preserved eclogitic assemblages, and of several decametre-size bodies with rare relics of the eclogite facies metamorphism.

Primary intrusive contacts between metagabbros and metapelites have not been identified, but intrusive relationships between metagabbros and orthogneisses occur near Alpe Arzola in the

Ribordone Valley, where medium-grained eclogitic metagabbros lenses are cut and enveloped by fine-grained aplitic-dykes (Fig. 3c, d). These outcrops suggest that metagabbros are older than orthogneisses as already shown by Biino & Pognante (1989) in the southern part of the Gran Paradiso Massif.

3. Petrography and mineral chemistry

In order to constrain the metamorphic evolution of the eastern border of the Gran Paradiso Massif, about thirty samples (metabasites and micaschists) were studied, from which two samples have been selected for thermodynamic modelling: a partially re-equilibrated eclogitic metagabbro (GMG10) and a Gln-Grt bearing micaschist (GMG2). On the basis of micro-structural relationships and mineral chemistry three Alpine metamorphic stages have been distinguished (Table 1): i) the peak-pressure metamorphic event (M1); ii) a first decompressional event (M2) developed in the eclogite facies and iii) the tectono-metamorphic event (M3) responsible for the development of the main regional foliation under upper greenschist to amphibolite facies conditions.

Minerals were analyzed with a Cambridge SEM-EDS with an accelerating voltage of 15 kV and 60 s counting time. X-ray element maps were acquired with the same accelerating potential as spot analyses with a counting time of 15 hours and a resolution of 512 x 415 pixels. Mineral formulae were recalculated assuming all measured FeO as Fe^{2+} except for clino-pypoxenes and amphiboles, for which Fe^{3+} were calculated according to Lindsley & Anderson (1983) and according to the IMA-97 (Leake *et al*., 1997) recommendation, respectively. Almost all amphibole chemical formula calculations show that the results of the *all ferrous* procedure satisfies charge balance and site occupancies, therefore all Fe measured by SEM-EDS is assumed to be Fe^{2+}. Representative mineral compositions are given in Tables 2 and 3.

Bulk rock compositions have been determined by XRF analyses at the Vancouver laboratories of the ALS Chemex (Table 4). Sample GMG10 shows a bulk-composition similar to the rocks

studied by Biino and Pognante (1989) in the southern part of the Gran Paradiso Massif, while sample GMG2 is a typical Na-Ca rich pelite.

3.1. Metagabbro (GMG10)

Eclogite facies assemblages are only preserved within the main metagabbro body outcropping near Alpe Arzola (Fig. 2) while smaller lenses have been completely re-equilibrated during the development of the regional foliation under upper greenschist to epidote-albite amphibolite facies conditions. According to micro-structural relationships the HP minerals can be related to two different eclogite facies metamorphic stages. The first (M1) event is defined by OmpI + Grt + Gln + Phe + Qtz + Tlc + Rt + Lws, now completely pseudomorphically replaced by Pg + Zo + Qtz. OmpI occurs as medium-grained (up to 5-6 mm) omphacite porphyroclasts surrounded by fine-grained garnet (Figs. 4e and 5a). Garnet idioblasts are small (100-150 μm) and occur around OmpI or as inclusions in amphibole, paragonite and zoisite. Aggregates of Zo + Pg + Qtz show rectangular or rhombohedral shapes and are interpreted as pseudomorphs after Lws (Figs. 4e, f and 5b). Tlc + Qtz + Rt occur as small inclusions within OmpI (Fig. 5c) while garnet includes only Qtz + Rt (Fig. 5d). The second metamorphic stage (M2) overprints M1 and represents the main assemblage preserved in the metagabbros. It consists of OmpII + Zo + Grt + Gln + Phe + Pg + Qtz + Rt. OmpII occurs as granoblastic aggregates within the rock matrix or as sub-grains grown at the expense of OmpI. Both omphacite generations are replaced by Act + Ab symplectites.

The regional foliation in well re-equilibrated rocks is defined by an assemblage of Act + Zo + Pg + Phe + Chl + Ab + Qtz + Rt (M3 event; sample GMG5 in Fig. 4d). Finally albite after white mica, biotite after phengite and hornblende at the rim of actinolite occur. In this paper only the two eclogite facies stages (M1 and M2) have been investigated by numerical modelling.

3.1.1. Garnet

Garnet preserves a growth zoning (Fig. 6a) characterized by decreasing Alm content, increasing Prp content, while the Grs component first increase from core to mantle and then decreases towards the rim (Fig. 6a). Three representative compositions can be distinguished: $Alm_{61-62}Grs_{23-24}Prp_{12-14}$ (core), $Alm_{55-56}Grs_{29-30}Prp_{12-14}$ (mantle), $Alm_{54-56}Grs_{23-25}Prp_{19-21}$ (rim). Sps is below 1-2 mol. % and does not reveal zoning. Some garnet shows an Alm-rich rim ($Alm_{61-62}Grs_{15-16}Prp_{20-21}$; Fig. 6.a) which is probably related to post peak re-equilibration and diffusion. This Alm-rich composition will not be used in pseudosection modelling. Garnets preserved as inclusions in other minerals show a large compositional range ($Alm_{53-58}Grs_{17-30}Prp_{15-26}$) overlapping the composition of garnet grown in contact with OmpI (Fig. 6b).

3.1.2. Omphacite

Pale green omphacite occurs both as 5 to 6 millimeters porphyroclasts (OmpI) and as small recrystallized grains and sub-grains of 20-40 μm (OmpII) grown at the expense of the first generation (Figs. 4b and 5a). OmpI has higher Jd contents (XJd 0.44-0.53) and small amounts of Acm (less than 5 mol. %), while OmpII has lower Jd contents (XJd 0.36-0.41) and Acm contents generally less than 9 mol. % (Fig. 6c). The $XMg(_{Fetot})$, defined as $Mg/(Mg+Fe_{tot})$, is 0.78-0.88 for OmpI and 0.72-0.87 for OmpII while $XMg_{(Fe2+)}$ is 0.85-0.92 for OmpI and 0.81-0.93 for OmpII.

3.1.3. White mica

White mica is widespread in the matrix and mainly consists of paragonite and minor phengite. Pg has an XNa (Na/(Na+K)) in the range of 0.80-0.90 and Phe shows decreasing Si a.p.f.u. contents from core (3.59 a.p.f.u on the base of 11 oxygens) to rim (3.37 a.p.f.u.). This change is associated to decreasing $XMg(_{Fetot})$ (core 0.90; rim 0.70) and increasing XNa (0.00-0.12 a.p.f.u.) (Fig. 6d). Rarely, small grains of margarite intergrown with Qtz + Phe have been observed at the interface between Zo and Omp, and are probably related to the destabilization of Zo.

3.1.4. Amphibole

Two amphibole generations can be distinguished. AmI is zoned (Fig. 6f), with a colourless to pale-blue Gln core with inclusions of Grt, and a green Act rim. The actinolitic rim has the same composition as the core of AmII which defines the main regional foliation. Gln has 1.70-1.85 $Al^{[VI]}$ a.p.f.u., 1.60-1.85 $Na^{[B]}$ a.p.f.u., 0.00-0.05 $Na^{[A]}$ a.p.f.u. Act has 0.20-0.49 $Al^{[IV]}$ a.p.f.u., 0.30-0.65 $Al^{[VI]}$ a.p.f.u., 0.20-0.45 $Na^{[B]}$ a.p.f.u., 0.15-0.25 $Na^{[A]}$ a.p.f.u. XMg is constant around 0.73-0.84 for both Gln and Act. Finally, both AmI and AmII show a rim of Hbl (0.50-1.10 $Al^{[IV]}$ a.p.f.u., 0.60-1.00 $Al^{[VI]}$ a.p.f.u., 0.20-0.45 $Na^{[B]}$ a.p.f.u., 0.25-0.45 $Na^{[A]}$ p.f.u) with 0.60-0.70 XMg (Figs. 5a and 6e, f). When Grt is in contact with Gln there is no reaction rim indicating textural equilibrium with Grt and Gln. Instead when Grt is in contact with AmII, garnet is resorbed and AmII shows a tschermakitic composition (Fig. 6e) suggesting disequilibrium between the two minerals.

3.1.5. Others minerals

Zoisite is represented by millimetric unzoned grains or aggregates (Fig. 4e-f) with constant Fe^{3+} around 0.08 a.p.f.u.; it is tightly intergrown with quartz, is associated with paragonite and locally contains omphacite inclusions. This Pg + Zo + Qtz association, often with a lozenge shape, is interpreted as pseudomorphs after Law + Omp with high Jd content (Fig. 4e, f), and confirm that Pg is stable in the HP stage as pointed out by Biino and Pognante (1989). Albite is associated to Act/Hbl within the re-equilibrated portions of the rock and has XAb > 0.91.

3.2. Metapelite (GMG2)

Sample GMG2 is characterized by a bi-modal distribution of garnet-size (Fig. 5e, f) shows a very well preserved HP pre-S_1 foliation (S_{HP}) defined by PheII + Qtz + Gln + Rt (Figs. 4b, c and 5g). White mica (PgI + PheI) defining a relict foliation (pre-S_{HP} in Fig. 5g) is preserved as high angle porphyroclasts respect to the eclogitic foliation (S_{HP}). An assemblage consisting of PheIII +

PgII + Hbl + Zo + Ab has mostly statically overgrown the eclogite facies foliation, but locally defines low-angle shear bands (Fig. 4c). These surfaces represent the regional foliation S_1, which is well developed in more pervasively re-equilibrated rocks (sample GMG17 in Fig. 4a). Particularly, PgII flakes have inclusions of Rt, Gln and matrix Grt, indicating that they grew after the pressure-peak assemblage and are often in aggregates with Zo, probably representing pseudomorphs after Lws. Finally, Chl and fine-grained Bt grew at the expense of Phe + Gln + Grt (Figs. 4b and 5h).

Two different garnet types can be distinguished on the basis of textural relationships and bi-modal grain-size distribution. The first (Fig. 5e) consists of up to 1.5 mm porphyroclasts showing an inclusion-rich core (GrtI) overgrown by an inclusion-poor rim (GrtII). The second type of garnet (Fig. 5f) occurs in the matrix, has smaller dimensions (300-350 μm) and few inclusions, leading us to interpret it as GrtII. Backscattered electron images reveal that both garnet types are irregularly overgrown by a rim of inclusion-free and homogeneous GrtIII maximum 50 μm thick (Figs. 5e, f).

3.2.1. Garnet

Textural distinction of the three garnet generations is confirmed by qualitative X-ray maps. The Ca map (Fig. 7c) is especially informative and shows that the GrtI-GrtII interface is characterized by a chemical discontinuity. A chemical profile through type-I garnet (Fig. 7a) shows that at this interface, Fe and Mg decrease, whereas Ca sharply increases and Mn slightly increases, indicating partial resorbtion of GrtI, also supported by its sub-idiomorphic and rounded shape. The contact between GrtII and GrtIII appears undisturbed at first sight (Figs. 5e, 7c), but close inspection of this boundary in backscattered electron images (Fig. 5f) shows that before the GrtIII growth, GrtII is partially resorbed and fractured. These fractures are subsequently healed by a garnet with a composition similar to that at the interface between GrtII and GrtIII (Fig. 5f). GrtIII is not present as individual neoblasts in the rock matrix.

Fig. 7a, b exhibits two representative close-spaced quantitative profiles of type-I porphyroclastic garnet (GrtI + GrtII + GrtIII) and of type-II garnet from the matrix (GrtII + GrtIII),

respectively. GrtI shows a continuous chemical zoning showing Alm and Prp increasing towards rim coupled to Grs and Sps decreasing. It is characterized by a core composition with $Alm_{58-60}Grs_{25-26}Prp_{6-7}Sps_{9-10}$ a mantle with $Alm_{64-69}Grs_{12-16}Prp_{14-16}Sps_{4-6}$ and a rim with $Alm_{70-71}Grs_{7-8}Prp_{17-18}Sps_{3-4}$. GrtII grown on GrtI porphyroclasts (Fig. 5e) shows decreasing Sps and Grs contents and increasing Prp towards the rim, whereas Alm first increases and then decreases (Fig. 7a). The core composition is $Alm_{69-71}Grs_{10}Prp_{15-16}Sps_{4-5}$ and the rim is $Alm_{69-71}Grs_{8-9}Prp_{21-22}$ Sps_{0-1}. Matrix garnet has a similar chemical zoning to GrtII, even if the core composition is slightly different ($Alm_{73-74}Grs_{10-11}Prp_{12-13}Sps_{3}$), probably because of off-core sectioning of either or both crystals. Finally, the discontinuous GrtIII is chemically unzoned (Fig. 7a) with an average composition of $Alm_{60-63}Grs_{28-31}Prp_{7-9}Sps_{0-2}$.

Inclusions are abundant in GrtI and consists of Qtz + Wm + Chl + Rt + Ap; GrtII includes only Qtz + Rt and GrtIII is free of inclusions.

3.2.2. White mica

White mica defining pre-S_{HP} consists of PgI flakes with minor PheI with 3.39-3.40 Si a.p.f.u.. On the basis of micro-structural relationships and chemical composition this pre-S_{HP} surface has been interpreted as a prograde Alpine foliation. The pre-S_1 HP foliation is defined by fine-grained PheII which has up to 3.50-3.55 Si a.p.f.u. in the core and at least 3.33 Si a.p.f.u. at the rim, while $XMg_{(Fetot)}$ decreases from 0.90 to 0.69 (Fig. 7d). Shear bands related to S_1 are defined by PgII and PheIII with 3.33-3.38 Si a.p.f.u., a composition similar to the rim composition of PheII. PgII is also present as millimetric porphyroblasts overgrowing the pre-S_1 foliation and has inclusions of Rt, Gln and Grt ($Alm_{72-74}Grs_{8-9}Prp_{18-20}$) with a composition similar to the GrtII rim. PgI and PgII are similar in composition.

3.2.3. Amphibole

AmphiboleI defining the pre-S_1 HP foliation is glaucophane and is rimmed by hornblende (amphiboleII) (Figs. 5h and 7e, f). Hbl is also present along shear bands that cut the HP foliation and defines the regional foliation S_1. Gln has 1.75-1.95 $Al^{[VI]}$ a.p.f.u., 0.00-0.20 $Al^{[VI]}$ a.p.f.u., 1.65-1.95 $Na^{[B]}$ a.p.f.u., with XMg decreasing from core (*ca* 0.80) to rim (*ca* 0.56). Hbl has 0.55-1.15 $Al^{[IV]}$ a.p.f.u., 0.55-1.10 $Al^{[VI]}$ a.p.f.u., 0.10-0.50 $Na^{[B]}$ p.f.u, 0.15-0.35 $Na^{[A]}$ a.p.f.u., 0.50-0.62 XMg. Gln is partially replaced by Qtz + Chl and by a symplectite consisting of Bt and probably of Chl (the darker mineral in the symplectite of Fig. 5h). The Gln core systematically shows a cation deficiency (generally in the range 0.05-0.10 a.p.f.u.) in the B site probably because of the presence of Li as already reported by Ungaretti et al., (1981) for some Gran Paradiso whiteschists or because of the presence of other elements in concentration below the detection limit (0.2 wt. % for a 60s counting time).

3.2.4. Other minerals

Albite poikiloblasts show very low An content (max 0.05 XAn), zoisite/clinozoisite grew after the pre-S_1 foliation and has 40-45 mol. % of Ep content corresponding to 7 wt. % Fe_2O_3. Finally, chlorite consists of fine-grained aggregates mainly at the expense of Hbl and shows a constant XMg around 0.46-0.52.

4. P-T conditions estimated from numerical modelling

Metamorphic conditions for the Gneiss Minuti Complex of the Gran Paradiso Massif in the Orco Valley have been reconstructed by combining micro-structural observations, chemical analyses and PT pseudosection modelling of the metagabbro (GMG10) and the metapelite (GMG2) samples described above. All pseudosections have been calculated with PERPLE_X (Connolly, 1990; Connolly & Petrini, 2002) using the thermodynamic database of Holland & Powell (1998, 2002 update). All Fe was considered as ferrous (except for GrtIII in metapelite), and H_2O was used

as a saturated pure fluid-phase (i.e. $a H_2O=1$). This is a realistic assumption for the studied samples since they contain abundant hydrous phases and because of the absence of carbonates and sulphides. The following solid solution models have been used: biotite (Tajcmanova et al., 2009), garnet (White et al., 2007), clinopyroxene (Green et al., 2007), amphibole (Dale et al., 2005), feldspar (Holland & Powell, 2003), paragonite (Chetterjee & Froese, 1975), phengite-muscovite, chlorite, talc, chloritoid, staurolite and carpholite (Holland & Powell, 1996, 1998).

A correct determination of the effective bulk chemical composition (e.g. Stüwe, 1997; Marmo et al., 2002; Evans, 2004) is very important to obtain the correct PT conditions of equilibration. Any mineral representing a relic of a previous metamorphic event does not contribute to the effective bulk chemical composition of the system. To determine the metamorphic conditions during growth of the three different garnet generations in sample GMG2, fractionation of bulk rock composition has been considered using the method of Gaidies et al. (2006, with ref. therein). For other minerals, chemical fractionation of the bulk composition has been calculated removing the average composition of each mineral increased by its volume proportion. The thermodynamically relevant bulk compositions used to calculate the different pseudosections are reported in Table 4. In all pseudosections, capital letters indicate solid solution models and small letters indicate pure phases; fields of di-, tree-, quadri- and penta-variant mineral assemblages are represented from white to dark grey hues.

4.1. Results for pseudosection modelling I (metagabbro GMG10)

The metamorphic assemblage for the eclogitic P-peak conditions (M1: OmpI + Grt + Gln + Lws + Phe + Tlc + Qtz + Rt) and the following re-equilibration stage during exhumation (M2: OmpII + Zo + Grt + Gln + Phe + Pg + Qtz + Rt) were modelled in pseudosection 1 in the PT range of 20-30 kbar and of 530-630 °C (Fig. 8). Since both Grt and OmpI have Qtz inclusions, calculations were done with SiO_2-saturated conditions. For the eclogite facies peak-conditions, it

was not possible to establish representative modal contents of minerals because the peak assemblage is preserved in 40-50 vol. % of the rock with OmpI porphyroclasts representing 20-25 vol. %. For this reason our results are only based on the minerals chemistry and on the metamorphic assemblages and not on modal abundances.

The pseudosection is contoured for Prp-Grs-Alm isopleths for garnet core ($Alm_{61-62}Grs_{23-24}Prp_{12-14}$), mantle ($Alm_{55-56}Grs_{29-30}Prp_{12-14}$) and rim ($Alm_{54-56}Grs_{23-25}Prp_{19-21}$) compositions (Fig. 8b), XJd and $XMg_{(Fetot)}$ in omphacite (Fig. 8c) and for Si a.p.f.u. in phengite and H_2O wt. % content (Fig. 8d).

According to the measured growth zoning, garnet grew during increasing T from 565 to 600 °C while P first decreases from 27.5 to 24.5 kbar and then increases again to 25.5-26.5 kbar (Fig. 8b). Garnet growth zoning lies in the Omp + Phe + Gln + Tlc + Lws + Qtz field that represent the inferred metamorphic assemblage M1 developed during the eclogitic peak metamorphic event. The Grt core should be in equilibrium with Phe showing 3.65-3.67 Si a.p.f.u. while the maximum measured content is 3.59 Si a.p.f.u. Garnet growth zoning isopleths suggest a drop in P followed by a further increase during prograde eclogite facies metamorphism up to *ca* 26.5 kbar at 600°C (Fig. 8). Since garnet grew around millimetric Omp and because there is no evidence of dynamic recrystallization under eclogite facies conditions, indeed no pre-S_1 foliation was developed in metagabbros which still preserves the magmatic structure, it is possible that the core represents a local equilibrium. The garnet core probably formed along the prograde path but owing to low diffusion of elements in absence of deformation, the bulk rock was not fully reacting and hence the core to mantle path may be meaningless. Instead, along the prograde path reconstructed for the mantle to rim garnet zoning omphacite shows increasing XJd (0.45-0.52) and increasing XMg (0.76-0.83) and the Si content in phengite diminishes from 3.58 to 3.47 a.p.f.u. in agreement with the measured OmpI and Phe compositions (Fig. 8c, d). The effect of Grt core and mantle fractionation was evaluated in Fig 8e, f and the comparison with Fig. 8b shows that the fractionation effect does not cause any appreciable shift in the Grt contours. This means that the position of the

garnet isopleths is not very sensitive to the change of the effective bulk composition and therefore, the unfractionated bulk composition can be used to evaluate the PT conditions for the prograde path.

With respect to the calculated assemblage, Gln, Grt, Omp and Phe are abundant in the preserved eclogitic portions of the rock, while Tlc is rare and Lws absent. Tlc, which is only preserved as inclusions in OmpI (Fig. 5c), is predicted to be 13-14 vol. % at peak P conditions, but owing to its mechanical properties it is an excellent candidate to accommodate deformation and so may be easily destabilized during the development of the regional foliation. The absence of Lws can be justified by inferring reaction with omphacite and transformation to zoisite + paragonite + quartz, as suggested by microstructural evidence (Figs. 4e, f). Lawsonite can be preserved only if exhumation occurs within its stability field, i.e. along an exhumation trajectory similar to the burial path (Zack et al., 2004, Clarke et al., 2006).

Numerical modelling yielded no stability field corresponding to the observed M2 eclogitic assemblage (OmpII + Zo + Grt + Gln + Phe + Pg + Qtz) because paragonite is never stabilized at HP conditions in pseudosection I (Fig. 8). The lack of Pg as product of the Lws-breakdown reaction may be related to the inaccuracy of the thermodynamic solution model of amphibole (Dale et al., 2005) or because the pseudomorphs after Lws represents a local equilibrium. On the other hand the Lws-out reaction curve for the pure end-member reported in bold in Fig. 8b shows that paragonite is a product of the reaction Jd + Lws = Pg + Zo + Qtz (Heinrich & Althaus, 1998). In addition, the computed Gln composition does not agree with measured one and is shifted towards Fe-enriched composition (modelled XMg=0.50-0.70 *vs* measured XMg=0.73-0.84). Such considerations, mainly the uncertainties in the amphibole solution model, may thus explain the presence of Act (winchite in composition) in the pseudosection instead of Pg in the Omp + Grt + Act + Gln + Phe + Zo + Qtz field. Therefore, the field with the asterisk (Fig. 8b) located at $P < 21.5$ kbar at T of 580-610°C may represent the PT conditions for the formation of Pg + Zo + Qtz pseudomorphs after Lws which, according to micro-structural data post-dated the HP peak conditions.

In summary, PT data obtained by pseudosection I constrain the early-stage of the PT path followed by the Gneiss Minuti Complex of the Gran Paradiso Massif in the Orco Valley. Specifically, the subduction event took place along a 6 °C/km up to a metamorphic peak of about 27 kbar at ca. 600 °C. During burial the H_2O content (structurally bounded in minerals) decreased from 4 to 3 wt. % and during the decompression it further decreased to 1-2 wt. % (Fig. 8d). The eclogitic metamorphic peak is inferred to be followed by a near-isothermal decompression step from 26-26.5 to 21-21.5 kbar at a constant temperature of 590-600 °C.

4.2. Results for pseudosection modelling II (metapelite GMG2)

The selected metapelite sample contains multistage garnet that was used to infer i) the polymetamorphic nature of the Gran Paradiso basement in the Orco Valley and ii) to better constrain the PT path followed by this unit during the Alpine HP tectono–metamorphic evolution.

In pseudosection modelling some problems arose from the amphibole solution model. The very high modal proportion of glaucophane calculated (*ca.* 35 vol. %) for sample GMG2, seems to be too large for a rock of pelitic composition; on the contrary the amount of Gln in our sample has been estimated as 21-23 vol. % by image analysis and qualitative optical investigation. Moreover, compositions modelled for glaucophane are different from those measured. The modelled phengite composition (maximum 0.01 Na a.p.f.u) differs from that measured (up to Na 0.10 a.p.f.u), too. This problem can be related to the inaccuracy of the solution model to predict the phengite-paragonite solvus at the K-rich side and contributes to overestimate the abundance of glaucophane. Indeed, if the white mica solution model would allow more Na in its lattice, the vol. % amount of Na-amphibole at HP conditions would be reduced.

4.2.1. PT conditions for GrtI

On the basis of micro-structural evidence GrtI porphyroclasts represent the oldest garnet generation preserved in our sample. Since GrtI porphyroclasts preserve the growth zoning, it has been possible to evaluate the PT conditions for its growth (Fig. 9). Isopleths intersection shows that garnet I core ($Alm_{58-60}Grs_{25-26}Prp_{6-7}$) is stable at ca 560 °C and 8 kbar in the field defined by the Chl + Phe(Ms) + Gln + Hbl + Pl + Grt + Qtz assemblage (Fig. 9b). GrtI mantle ($Alm_{64-69}Grs_{12-16}Prp_{14-16}$) equilibrated at ca 610 °C and 9 kbar corresponding to the stability field of the assemblage Bt + Chl + Pl + Grt + Qtz + Pg while the rim does not show a good intersection. Along the slightly compressional prograde trajectory modelled on the basis of garnet zoning, Gln + Hbl + Phe(Ms) disappeared, Chl is almost totally consumed, while Bt grew up to 19-20 vol. %. The modelled composition of Gln in equilibrium with GrtI core is Fe-rich and is probably related to an overestimation of the Gln stability field towards low pressure. In Fig. 9c, d the effect of the Grt core and mantle fractionation is investigated but there is no significant change in the garnet isopleths intersection.

It is worth of note that the calculated metamorphic assemblages in equilibrium with GrtI correspond to upper amphibolite facies metamorphic conditions; the occurrence of inclusions of Qtz + Ms + Chl in GrtI is also compatible with the calculated trajectory, that can be thus referred to a pre-Alpine metamorphic history. The absence of other pre-Alpine mineralogical relics in GMG2 is related to overprinting processes during the Alpine metamorphic cycle. The occurrence of pre-Alpine garnet porphyroclasts was already reported from other localities of the Gran Paradiso Massif (e.g., Borghi & Sandrone, 1995; Le Bayon et al., 2006).

4.2.2. PT conditions for GrtII

Garnet II grew both rimming GrtI and in the matrix and shows textural equilibrium with PheII + Gln + Qtz + Rt defining the M1 Alpine metamorphic assemblage, which is syn-kinematic to the S_{HP} foliation development. Because a pre-eclogitic foliation, defined mainly by paragonite and related to the burial stage is preserved (pre-S_{HP} of Fig. 5g), garnet I and paragonite I fractionation

must be considered to constrain the reactive bulk composition during the growth of GrtII. In order to evaluate the amount of Pg stable during the pre-eclogitic stage, the pseudosections of Fig. 10a, b has been calculated. It allowed to establish the volume fraction of relict paragonite related to the pre-eclogitic stage and to calculate the effective bulk chemical composition for the evaluation of GrtII growth conditions. The vol. % of paragonite fractionated during burial is directly related to the variation of the system bulk composition and has been reported on the x-axis of Fig. 10 a, b. The lower left corner represents the rock composition with GrtI fractionated. The y-axis represents a 6 °C/km subduction gradient expressed as P(T) and was calculated assuming an average density of 2.95 kg/dm^3 for a subducted crust. The 6 °C/km geothermal gradient is justified by the PT conditions inferred from sample GMG10 (Fig. 8d). Compositional isopleths of GrtII core ($Alm_{69-71}Grs_{10}Prp_{15-16}$) intersects at around 25 kbar (corresponding to 520 °C for a gradient of 6 °C/km) for a bulk composition corresponding to a fractionation of 6.5 vol. % of paragonite (average composition: 7.55 Na_2O, 0.74 K_2O, 40.88 Al_2O_3, 50.53 SiO_2). The reactive composition used for the calculation of Fig. 10c, d (column I of Table 4) is derived subtracting 6.5 vol. % of Pg from the composition of column G in Table 4.

In Fig. 10b contours of Si a.p.f.u. for phengite are also reported. They show that for the established reactive composition (6.5 vol. % of Pg fractionated), the Si content in phengite increases with P(T) up to a maximum value of 3.52 a.p.f.u corresponding to a P of 23-24 kbar and then decreases down to 3.44 a.p.f.u. at 27 kbar from where it increases again. This indicates that prograde phengite grown during burial can reach a Si a.p.f.u. value higher than that stable at peak P conditions.

The pseudosection (Fig. 10c, d) has been calculated in the PT range of 20-30 kbar and 530-630 °C and Phe + Qtz + Rt are stable throughout the PT range. The intersection of garnet compositional isopleths indicate that GrtII core ($Alm_{69-71}Grs_{10}Prp_{15-16}$) grew at *ca.* 540°C and 25 kbar (Fig. 10c, d) in the Cp + Gln + Grt + Phe + Lws + Qtz, while the isopleths of the rim composition ($Alm_{69-71}Grs_{7-9}Prp_{21-22}$) crosses at 595 °C and 28.5 kbar in the Cs + Omp(Jd) stability

field which are both absent in our sample. In pseudosection of Fig. 10e the GrtII core composition was fractionated and the garnet rim isopleths run parallel to each other in the field Gln + Grt + Phe + Lws + Ky + Qtz/Cs. The absence of coesite inclusions in garnet and of quartz derived from its recrystallization suggests that metamorphic pressure remained below the coesite-in reaction (P < 27.5 kbar). Despite the parallelism between the garnet isopleths, it was possible to constrain PT conditions at 585-595 °C and 26-27.5 kbar in the Gln + Grt + Phe + Lws + Qtz + Ky field assemblage (M1 event, Fig. 10d). These conditions represent the eclogitic peak for sample GMG2. Garnet II rim grown at peak-P conditions is modelled to be in equilibrium with *ca.* 37 vol. % Gln, 23 vol. % Phe, 11 vol. % of Lws and less than 3 vol. % of Ky. Kyanite lacks in the sample but due to its low amount, it could have been completely consumed during decompression, especially during the development of the main regional foliation, or could have never formed. Lawsonite too is absent, but the presence of Zo with quartz inclusions associated to Pg overgrowing the pre-S_1 foliation could indicate the presence of a former Ca-rich phase, possibly lawsonite.

Isopleths for Si a.p.f.u. in Phe show that Phe in equilibrium with GrtII rim has up to 3.45 a.p.f.u., a value that is lower than the maximum value measured (3.55 a.p.f.u.). Such a high Si content could represent a relict of a previous prograde metamorphic event (Fig. 10b) or the solid solution model of phengite (Holland & Powell, 1998) overestimates pressure. The same problem arises also using the alternative solution model of Coggon & Holland (2002), for which the pressure overestimation is even larger (3.40 Si a.p.f.u. at 595 °C and 27.5 kbar). Since the modelled isopleths for Si in Phe are similar using different solution models, the first hypothesis is thought to be correct and Phe with 3.45-3.55 Si a.p.f.u. is related to the prograde path.

The GrtII core to rim composition allowed to reconstruct a prograde and compressional PT path along which Cp is consumed and Grt + Phe + Gln grew at its expense. The PT trajectory is nearly parallel to the 6 °C/km geothermal gradient and similar to the PT path reconstructed for sample GMG10 (Fig. 10e). The subsequent decompressional stage is constrained by the assemblage Grt + Gln + Phe + Pg + Qtz + Zo (M2 event) which corresponds to the starred stability field in Fig.

10d, at about 21-22 kbar and 590-610 °C. The transition from the M1 to the M2 assemblage is marked, as in the metagabbro sample, by the breakdown of Lws, which is very difficult to preserve. Garnet on the other hand, even if in low amount (4-5 vol. %) is well preserved and Gln is preserved because of its abundance in the rock (21-23 vol. %) and because of its large stability field throughout the pseudosection.

4.2.3. PT conditions for GrtIII

The growth of a further garnet generation over GrtII has been interpreted on the basis of micro-structural relationships as a new generation and therefore called GrtIII. To constrain the effectively reacting bulk composition during the growth of GrtIII (Fig. 11) fractionation of GrtI, GrtII, Gln and Phe has been considered because they are preserved in high amount (21-23 vol. % and 20-22 vol. % respectively) contributing to the fractionation of the bulk rock composition. The reacting bulk chemical composition (Table 4, column M) has been calculated by fractionating 22 vol. % of Gln and 21 vol. % of Phe taking the average composition of both Gln (7.56 Na_2O, 0.46 CaO, 8.67 FeO, 10.80 MgO, 12.16 Al_2O_3, 60.87 SiO_2) and Phe with Si a.p.f.u. $\geq$ 3.40 (0.47 Na_2O, 11.15 K_2O, 2.01 FeO, 3.82 MgO, 28.13 Al_2O_3, 53.43 SiO_2).

Fig. 11 was calculated rejecting Gln from calculations because of the problem enhanced is section 4.1. Since the M3 assemblage contains Ep the additional component Fe_2O_3 was introduced in the system. Since Ep in equilibrium with M3 is in low amount (< 5 vol. %) and contains around 7 wt. % Fe_2O_3 we have introduced 0.25 wt. % Fe_2O_3 in the system which was subtracted from the whole FeO. The presence of Fe^{3+} cause the stabilization of Mag at low pressure which is metastable with respect to Ilm. Moreover, the assemblages with two Hbl (hornblende s.s and barroisite) are probably metastable with respect to Gln. The compositional isopleths of GrtIII intersect at 600-625 °C and 9.5-11.5 kbar in the Phe + Hbl + Pg + Grt + Ep + Pl + Qtz stability field (Fig. 11b) and is in equilibrium with Hbl showing 0.52-0.58 XMg in agreement with the measured one (0.50-0.62

XMg) (Fig. 11c). The Chl composition XMg (0.46-0.52) would constrain the decompression to 560-580 °C and 7-8 kbar in the Chl + Phe + Hbl + Grt + Pg + Pl + Qtz (Fig. 11.c).

5. Discussion

Pseudosection modelling of HP relic assemblages preserved in two different chemical systems allowed to reconstruct a portion of the PT path followed by the Gran Paradiso Massif during the Alpine subduction. The metamorphic evolution of the Gneiss Minuti Complex from the Orco Valley is marked by three texturally distinct mineral assemblages, defining one pre-Alpine and three Alpine metamorphic events (M1, M2, M3) developed under different PT conditions (Tab. 1).

5.1. Pre-Alpine history

Relict Variscan garnet defines a prograde path from 560°C to 620°C at 8-9 kbar. Other evidence of the pre-Alpine nature of the Gneiss Minuti Complex in the Orco Valley area is represented by the preservation of the magmatic texture in metagabbros (omphacite crystals grown directly on magmatic clinopyroxene sites) which suggest that these gabbros intruded a HT basement during the first stage of the Variscan magmatic cycle before the intrusion of the Late Variscan granitoids dated at 265-275 Ma (Bertrand et al., 2000; Bertrand et al., 2005; Ring et al., 2005).

5.2. Alpine history

The first Alpine metamorphic event M1 occurred under eclogite facies conditions at 26-27 kbar and 580-600 °C and is characterized by the assemblage OmpI + Grt + Gln + Lws

(pseudomorphs after it) + Phe + Tlc + Qtz in the basic system and the assemblage Gln + GrtII + PheI + Qtz + Lws (pseudomorphs after it) + Ky (inferred) + Rt in the pelitic system.

Peak-pressure conditions higher than those estimated by previous works (Wei & Powell, 2003, 2004; Meffan-Main et al., 2004; Le Bayon et al., 2006) have been thus inferred for the Alpine eclogitic peak in the eastern portion of the Massif. Maximum PT estimates of 21–23 kbar and 540–570 °C, registered by whiteschist shear bands within the orthogneisses, have been reported by Wei and Powell (2003, 2004) and by Meffan-Main et al. (2004) in the south-westernmost part of the Massif (Bonneval) and in the northern part (Cogne Valley), respectively. Peak-eclogitic PT conditions of 18-19 kbar at 490-510°C have been reported by Le Bayon et al. (2006) for a garnet-chloritoid bearing micaschist from Cogne Valley.

The garnet growth zoning of the metagabbro sample GMG10 records a drop in P followed by a further increase during prograde eclogite facies metamorphism up to *ca* 26.5 kbar at 600°C (Fig. 8). The garnet core should be in equilibrium with phengite with 3.65-3.67 Si a.p.f.u. while measured phengite has maximum 3.59 Si a.p.f.u. Moreover, since garnet grew around millimetric Omp and because evidence of dynamic recrystallization is absent, it is possible that the garnet core represents a local equilibrium affected by low diffusion of elements. In this case, the core to mantle growth zoning does not represent a true PT path and must not be considered further.

Both the basic and the pelitic sample record a second HP metamorphic event (M2) represented by the main assemblage preserved in the rocks (OmpII + Zo + Grt + Gln + Phe + Pg + Qtz + Rt in GMG10 and PheII + GrtII + Gln + PgI + Zo + Qtz + Rt in GMG2) and by pseudomorphs after Lws in the metagabbro (Zo + Pg + Qtz aggregates). The former presence of Lws in the metapelite sample GMG2 is less clear, but it is suggested by the presence of Zo + Qtz intergrowths grown over the HP foliation. Pseudosection modelling suggests average equilibration conditions of 21-22 kbar and 590-610 °C for the M2 event thus implying a nearly isothermal decompressional evolution from M1 to M2 (Fig. 12).

Finally, the M3 metamorphic event is syn-kinematic with respect to the development of the regional foliation defined by the assemblage GrtIII + PheIII + PgII + Hbl + Qtz + Ab + Ep + Rt in the metapelite which was equilibrated at ca 600-625°C and 9.5-11.5 kbar. The equivalent assemblage in metagabbros is represented by Act + Zo/Ep + Phe + Pg + Chl + Qtz + Ab + Rt.

In Fig. 12 the complete Alpine PT path inferred for the eastern side of the Gran Paradiso Massif is reported. The good agreement between predicted and observed phase assemblages and phase compositions supports the assumptions made for constructing the pseudosections and suggests that the reconstructed PT path represents a good approximation of the PT evolution of the eastern Gran Paradiso Massif.

5.3. Exhumation mechanisms

The PT path reconstructed in this work shows a clockwise trajectory, characterized by a prograde stage along a 6°C/km geotherm up to the eclogitic peak (M1 event). The exhumation path shows a decompression of at least 15-18 kbar which is isothermal or linked to a little T increase, during which the Lws-out decompressional reaction was crossed (M2 event), leading to the development of the main regional tectono-metamorphic event (M3). Therefore, the S_1 foliation equilibrated in a geodynamic setting characterized by an apparent geothermal gradient of about 14-17 °C/km.

In Fig. 12 the PT paths reconstructed by Borghi et al., (1996), Brouwer et al. (2002), Le Bayon et al. (2006) and Gabudianu Radulescu et al., (2009) have been included for comparison. The Alpine trajectory we have reconstructed does not support any late thermal pulse as previously proposed by Borghi et al. (1996) and by Brouwer et al. (2002) and a slightly decompressional heating could be possible as for the northern Gran Paradiso (Le Bayon et al., 2006). The differences between these PT paths and the trajectory reconstructed in this work could be explained by the

existence of a metamorphic field gradient or by the presence of different tectonic units as shown by Le Bayon & Ballèvre (2006) in the northern part of the Massif. Since the higher PT conditions are reported from the external part of the Gran Paradiso Massif (23-27 kbar and 580-600 °C; this work, Gabudianu Radulescu et al., 2009) compared to the PT path reconstructed for the inner portions (Brouwer et al., 2002; Le Bayon et al., 2006) we suggest the presence of different tectonic slices which experienced different PT path along the subduction channel.

The regional foliation S_1 developed during top-to-W compression regime (Gasco et al., 2009) and according to both metamorphic and structural relationships can be related to the top-to-NW shearing event dated at 38-40 Ma by Inger and Ramsbotham (1997) in the same area while the HP event (our pre-S_1 foliation) is dated at 43 Ma (Meffan-Main et al., 2004) in the northern portion of the Gran Paradiso. Recent geochronology (Gabudianu Radulescu et al., 2009) for the same outcrop dated by Meffan-Main et al., (2004) yield 33.7 ± 1.6 Ma for the eclogite facies stage which clearly overlap the age of the greenschist facies re-equilibration stage (33-40 Ma; Inger & Ramsbotham, 1997; Freeman et al., 1998; Meffan-Main et al., 2004) and the zircon fission tracks age (29-33 Ma; Hurford & Hunziker, 1989, Malusà & Vezzoli, 2006). Discussion about the true age of the HP metamorphism in the Gran Paradiso is beyond the scope of this paper, but for the reason exposed above the age determined by Gabudianu Radulescu et al., (2009) are not considered in our discussion. Comparing geochronological data from literature and thermobarometric data reported in this paper Gran Paradiso nappe was exhumed from 26-27 kbar (a minimum of 90-95 km) to 9-11 kbar (about 30-40 km) in a time range of 3-5 My implying average exhumation rates of 10-22 mm/y. For such high exhumation rates little thermal exchange can occur with the surrounding rocks, therefore the eclogite facies rocks can preserve the temperature of the peak pressure during exhumation (Hacker & Peacock, 1995). These high exhumation rates cannot be reached only by normal isostatic uplift or by erosion, but needs to be driven by extensional tectonic and/or by buoyancy forces (Burov et al., 2001). In this context is noteworthy that roughly 80-90 vol. % of the Gran Paradiso Massif is made up of orthogneisses and well preserved meta-granites with a density

of 2.7-2.9 kg/dm^3; these rocks have been subducted since contains lenses of whiteschists but did not equilibrate at HP conditions probably because of H_2O deficiency that prevents the activation of metamorphic reactions and recrystallization into denser rocks (Proyer, 2003) or, most probably, because deformation concentrated along the whiteschist bearing shear zones. At the depth of 90 km, we expect a density of 3.2-3.3 kg/dm^3 in surrounding rocks. This means a density contrast of 300-600 kg/m^3 and a high buoyancy effect (see discussion in Ranalli et al., 2005) acting on the continental crustal slice that is forced to return toward the base of the crust after delamination from the subducting slab. Therefore, the first exhumation stage is mainly controlled by a buoyancy effect from the eclogite facies stage to the development of the main regional foliation. At the base of the thickened crust (30-40 km) the density contrast is too low or vanished at all, the buoyancy effect ceased and other exhumation mechanisms must be invoked. Since Gasco et al. (2009) reported a post-S_1 extensional shear zone (Orco Shear Zone) at the top of the nappe-stack consisting of tectonic units that experienced eclogite facies metamorphism(Gran Paradiso Massif and Zermatt-Saas Unit), we suggest the presence of a second exhumation stage mainly driven by extensional tectonic.

6. Conclusions

Detailed mapping of the eastern border of the Gran Paradiso Massif (Gasco et al., 2009), combined with micro-structural and petrological investigation allowed to select suitable samples to reconstruct its polymetamorphic history.

In particular, three different Grt generations have been found in metapelite from Gran Paradiso Massif, as already suggested by Borghi et al. (1996). Garnet I composition and zoning suggest a prograde trajectory in the amphibolite facies, typical of the Variscan metamorphism. The second and the third garnet generations have been related to the Alpine metamorphic evolution:

GrtII to the eclogitic peak stage (M1) and GrtIII to the development of the main tectono-metamorphic event which is the regional foliation.

The relict Variscan garnet defines a prograde path from 560°C to 620°C at 8-8.5. Other evidences of the pre-Alpine nature of the Gneiss Minuti Complex in the Orco Valley area are represented by the preservation of the magmatic texture in metagabbros (omphacite crystals grown directly on magmatic clinopyroxene/hornblende sites) which suggest that these gabbros intruded an HT basement complex during the first stage of the Variscan magmatic cycle before the intrusion of the Late Variscan granitoids dated at 265-275 Ma (Bertrand et al., 2000; Bertrand et al., 2005; Ring et al., 2005).

Pseudosection modelling of the Alpine metamorphic assemblages from two different chemical systems, a metagabbro and a metapelite, allowed to reconstruct the Alpine PT path for the eastern side of the Gran Paradiso Massif: PT conditions very close to the quartz-coesite transition have been inferred, similarly to the PT estimations reported by Gabudianu Radulescu et al., (2009) for the whiteschists outcropping in the northern part of the massif. The HP peak stage was reached at 26-27 kbar for 580-600 °C along a subduction gradient of 6 °C/km and was followed by near-isothermal or slightly prograde exhumation to mid-crustal depths where the main regional foliation of the Gran Paradiso developed at ca 600-625°C and 9.5-11.5 kbar. This foliation equilibrated in a geodynamic setting showing a 14-17 °C/km apparent geothermal gradient (Fig. 12).

Further exhumation was related to major cooling up to shallow crustal levels. Comparing our Alpine PT path with those reported in literature for the Gran Paradiso Massif, the reconstructed Alpine trajectory does not support any late thermal pulse as previously proposed by Borghi et al. (1996) and by Brouwer et al. (2002) nor a slightly temperature increase during decompression (Le Bayon et al., 2006). On the other hand the PT path proposed in this work is similar to that reported by Ballèvre (1988).

The high exhumation rates inferred by geochronological data present in literature (Inger & Ramsbotham, 1997; Meffan-Main et al., 2004) are in agreement with our PT path and can be

explained by buoyancy forces (Burov et al., 2001) up to the base of the crust. Since Gasco et al. (2009) reported pervasive top to W shearing during the development of the main foliation S_1 (M3 event) and because the subduction of the European margin towards E to SE under the African plate is commonly accepted (for review see Schmid et al., 2008), we suggest a first fast exhumation stage mainly driven by buoyancy forces in a compressional regime from 90-95 km to 30-40 km. A second exhumation stage from the base of the orogenic wedge towards shallow crustal levels was related to major cooling and was mainly controlled by extensional tectonics along the Orco Shear Zone (Gasco et al., 2009).

Acknowledgments

We are grateful to J.A.D. Connolly (ETH, Zurich) and to C. Groppo (University of Torino) for the useful suggestions during pseudosections modelling and to B. Lombardo (CNR, Torino) and R. Compagnoni (University of Torino) for fruitful discussions on the Gran Paradiso geology. Constructive revision from F. Brouwer and J. Hermann is greatly appreciated. This work was financially supported by Ministero dell'Università e della Ricerca Scientifica e Tecnologica (M.U.R.S.T.).

References

Ballèvre, M., 1988. Collision continentale et chemins P–T: L'unité pennique du Grand Paradis (Alpes occidentales). Mémoires et Documents du Centre Armoricain d'Etudes Structurales des Socles, 19, 1-352.

Bertrand, J.M., 1968. Étude structurale du versant occidental du Massif du Grand Paradis (Alpes Graies). Géologie Alpine, 44, 55–87.

Bertrand, J.M., Pidgeon, R.T., Leterrier, J., Guillot, F., Gasquet, D., Gattiglio, M., 2000. SHRIMP and IDTIMS U-Pb zircon ages of the pre-Alpine basement in the internal Western Alps (Savoy and Piedmont). Schweizerische Mineralogische und Petrographische Mitteilungen, 80, 225-248.

Bertrand, J.M., Pidgeon, R.T., Guillot, F. 2005. Permian zircon U-Pb ages in the Gran Paradiso massif: revisiting post-Variscan events in the Western Alps. Schweizerische Mineralogische und Petrographische Mitteilungen, 85, 15-29.

Biino, G., Pognante, U., 1989. Paleozoic continental-type gabbros in the Gran Paradiso nappe (Western Alps, Italy): Early-Alpine eclogitization and geochemistry. Lithos, 24, 3-19.

Borghi, A., Compagnoni, R., Sandrone, R., 1996. Composite PT paths in the internal Penninic massifs of the Western Alps: petrological constrains to their thermo-mechanical evolution. Eclogae Geologicae Helvetiae, 89, 345-367.

Borghi, A., Sandrone, R., 1995. Petrological constraints on the Alpine PT history of the internal Pennine nappes of the Western Alps. Bollettino del Museo Regionale di Scienze Naturali (Torino), Supplemento, 13, 241-272.

Brouwer, F.M., van de Zedde, D.M.A., Wortel, M.J.R., Vissers, R.L.M., 2004. Late-orogenic heating during exhumation: Alpine PTt trajectories and thermomechanical models. Earth and Planetary Science Letters, 220, 185-199.

Brouwer, F.M., Vissers, R.L.M., Lamb, W.M., 2002. Structure and metamorphism of the Gran Paradiso massif, Western Alps, Italy. Contributions to Mineralogy and Petrology, 143, 450-470.

Bucher, K., Frey, M., 2002. Petrogenesis of Metamorphic Rocks. Springer-Verlag, 7th edition, p. 335-336.

Burov, E., Jolivet, L., Le Pourhiet, L., Poliakov, A., 2001. A thermomechanical model of exhumation of high pressure (HP) and ultra-high pressure (UHP) metamorphic rocks in Alpine-type collision belts. Tectonophysics, 342, 113-136.

Callegari, E., Compagnoni, R., Dal Piaz, G.V., 1969. Relitti di strutture intrusive erciniche e scisti a sillimanite nel Massiccio del Gran Paradiso. Bollettino della Società Geologica Italiana, 88, 59-69.

Chatterjee, N.D, Froese, E., 1975. A thermodynamic study of the pseudobinary join muscovite-paragonite in the system $KAlSi_3O_8$ – $NaAlSi_3O_8$ – Al_2O_3 – SiO_2 – H_2O. American Mineralogist, 60, 985-993.

Clarke, G.L., Powell, R., Fitzherbert, J.A., 2006. The lawsonite paradox: a comparison of field evidence and mineral equilibria modelling. Journal of Metamorphic Geology, 24, 715-725.

Coggon, R., Holland T.J.B., 2002. Mixing properties of phengitic micas and revised garnet-phengite thermobarometers. Journal of Metamorphic Geology, 20, 683-696.

Compagnoni, R., Elter, G., Lombardo, B., 1974. Eterogeneità stratigrafica del complesso degli "Gneiss Minuti" nel massiccio cristallino del Gran Paradiso. Memorie della Società Geologica Italiana, 13, 227-239.

Compagnoni, R., Lombardo, B., 1974. The Alpine age of the Gran Paradiso eclogites. Rendiconti della Società Geologica Italiana di Mineralogia e Petrografia, 30, 223-237.

Compagnoni, R., Prato, R., 1969. Paramorfosi di cianite su sillimanite in scisti pregranitici del Massiccio del Gran Paradiso. Bollettino della Società Geologica Italiana, 88, 547-549.

Connolly, J.A.D., 1990. Multivariable phase diagrams: an algorithm based on generalized thermodynamics. American Journal of Science, 290, 666-718.

Connolly, J.A.D., Petrini, K., 2002. An automated strategy for calculation of phase diagram sections and retrieval of rock properties as a function of physical conditions. Journal of Metamorphic Geology, 20, 697-708.

Dale, J., Powell, R., White, R.W., Elmer, F.L., Holland, T.J.B., 2005. A thermodynamic model for Ca–Na clinoamphiboles in Na_2O–CaO–FeO–MgO–Al_2O_3–SiO_2–H_2O–O for petrological calculations. Journal of Metamorphic Geology, 23, 771-791.

Dal Piaz G.V., Lombardo, B., 1986. Early alpine eclogite metamorphism in the Penninic Monte Rosa-Gran Paradiso basement nappes of the north-western Alps. Geological Society of America Memoirs, 164, 249-265.

Elter, G., 1960. La zona Penninica dell'alta e media Valle d'Aosta e le unità limitrofe. Memorie degli Istituti di Geologia e Mineralogia dell'Università di Padova, 22, 1-114.

Elter, G., 1971. Schistes lustrés et ophiolites de la zone piémontaise entre Orco and Doire Baltée (Alpes Graies). Hypothèses sur l'origine des ophiolites. Géologie Alpine (Grenoble), 47, 147-169.

Elter, G., 1972. Contribution à la connaissance du briançonnais interne et de la bordure piémontaise dans les Alpes Graies nord-orientales et considérations sur les rapports entre les zones du briançonnais et des Schistes lustrés. Memorie degli Istituti di Geologia e Mineralogia dell'Università di Padova, 28, 1-20.

Evans, T.P, 2004. A method for calculating effective bulk composition modification due to crystal fractionation in garnet-bearing schist: implications for isopleth thermobarometry. Journal of Metamorphic Geology, 22, 547-557.

Freeman, S.R., Inger, S., Butler, R.W.H. & Cliff, R.A., 1997. Dating deformation using Rb-Sr in white mica: Greenschist facies deformation ages from the Entrelor shear Zone, Italian Alps. Tectonics, 16, 57-76.

Gabudianu Radulescu, I., Rubatto, D., Gregory, C. Compagnoni, R., 2009, The age of HP metamorphism in the Gran Paradiso Massif, Western Alps: A petrological and geochronological study of "silvery micaschists", Lithos, 110, 95-108.

Gaidies, F., Abart, R., De Capitani, C., Schuster, R., Connolly, J.A.D., Reusser E. 2006. Characterization of polymetamorphism in the Austroalpine basementa east of the Tauern

Window using garnet isopleth thermobarometry. Journal of Metamorphic Geology, 24, 451-475.

Gasco, I, Gattiglio, M., Borghi, A., 2009. Structural evolution of different tectonic units across the Austroalpine-Penninic boundary in the middle Orco Valley (Western Italian Alps). Journal of Structural Geology, 31, 301-314.

Green, E.C.R., Holland, T.J.B., Powell, R., 2007. An order-disorder model for omphacitic pyroxenes in the system jadeite-diopside-hedenbergite-acmite, with applications to eclogite rocks. American Mineralogist, 92, 1181-1189.

Hacker B.R. Peacock S.M. 1995. Creation, Preservation and Exhumation of UHPM Rocks. In: Coleman R.G. and Wang X (eds). Ultrahigh Pressure Metamorphism, Cambridge University Press, 159-181.

Heinrich, W., Althaus, E., 1998. Experimental determination of the reactions 4 lawsonite + 1 albite = 1 paragonite + 2 zoisite + 2 quartz + 6 H_2O and 4 lawsonite + 1 jadeite = 1 paragonite + 2 zoisite + 1 quartz + 6 H_2O. Neues Jahrbuch für Mineralogie Monatshefte, 11, 516–528.

Holland, T.J.B. & Powell, R., 1996. Thermodynamics of order-disorder in minerals 2. Symmetric formalism applied to solid solutions. American Mineralogist, 81, 1425-1437.

Holland, T.J.B., Powell, R., 1998. An internally consistent thermodynamic data set for phases of petrologic interest. Journal of Metamorphic Geology, 16, 309-343.

Holland, T.J.B., Powell, R., 2003. Activity–composition relations for phases in petrological calculations: an asymmetric multicomponent formulation. Contributions to Mineralogy and Petrology, 145, 492-501.

Hurford, A.J., Hunziker, J.C., 1989. A revised thermal history for the Gran Paradiso massif. Schweizerische Mineralogische und Petrographische Mitteilungen, 69, 319-329.

Inger, S., Ramsbotham, W., 1997. Syn-convergent exhumation implied by progressive deformation and metamorphism in the Valle dell'Orco transect, NW Italian Alps. Journal of the Geological Society of London, 154, 667-677.

Kretz, R., 1983. Symbols for rock-forming minerals. American Mineralogist, 68, 277-279.

Leake, B.E., Woolley, A.R., Arps, C.E.S., Birch, W.D., Gilbert, M.C., Grice, J.D., Hawthorne, F.C., Kato, A., Kisch, H.J., Krivovichev, V.G., Linthout, K., Laird, J., Mandarino, J.A., Maresch, W.V., Nickel, E.H., Rock, N.M.S., Schumacher, J.C., Smith, D.C., Stephenson, N.C.N., Ungaretti, L., Whittaker, E.J.W., Guo, Y., 1997. Nomenclature of amphiboles; report of the subcommittee on amphiboles of the International Mineralogical Association, Commission on New Minerals and Mineral Names. Canadian Mineralogist, 35, 219-246.

Le Bayon, B., Ballèvre, M., 2006. Deformation history of a subducted continental crust (Gran Paradiso, Western Alps): continuing crustal shortening during exhumation. Journal of Structural Geology, 28, 793-815.

Le Bayon, B., Pitra, P., Ballèvre, M., Bohn, M., 2006. Reconstructing PT paths during continental collision using multistage garnet (Gran Paradiso nappe, Western Alps). Journal of Metamorphic Geology, 24, 477-496.

Lindsley, D.H., Anderson, D.J. 1983. A two-pyroxene thermometer. Journal of Geophysical Research, 88A, 887-906.

Malusà, M.G., Vezzoli, G., 2006. Interplay between erosion and tectonics in the Western Alps. Terra Nova, 18, 104-108.

Marmo, B. A., Clarke, G. L., Powell, R., 2002. Fractionation of bulk rock composition due to porphyroblast growth; effects on eclogite facies mineral equilibria, Pam Peninsula, New Caledonia. Journal of Metamorphic Geology, 20, 151-165.

Meffan-Main, S., Cliff, R.A., Barnicoat, A.C., Lombardo, B., Compagnoni, R., 2004. A Tertiary age for Alpine high-pressure metamorphism in the Gran Paradiso massif, Western Alps: a Rb-Sr microsampling study. Journal of Metamorphic Geology, 22, 267-281.

Proyer, A., 2003. The preservation of high-pressure rocks during exhumation: metagranites and metapelites. Lithos, 70, 183-194.

Ranalli, G., Martin, S., Mahatsente, R., 2005. Continental subduction and exhumation: an example from Ulten Unit, Tonale Nappe, eastern AustroAlpine. Geological Society of London, Special Publications, 243,159-174.

Ring, U., Collins, A., S., Kassem, O., K., 2005. U-Pb SHRIMP data on the crystallization age of the Gran Paradiso augengneiss, Italian Western Alps: Further evidence for Permian magmatic activity in the Alps during break-up of Pangea. Eclogae Geologicae Helvetiae, 98, 363-370.

Schmid, S.M., Bernoulli, D., Fügenschuh, B., Matenco, L., Schefer, S., Schuster, R., Tischler, M., Ustaszewski, K., 2008. The Alpine-Carpathian-Dinaridic orogenic system: correlation and evolution of tectonic units. Swiss Journal of Geosciences, 101, 139-183.

Schmid, S.M., Fügenschuh, B., Kissling, E., Schuster, R., 2004. Tectonic map and overall architecture of the Alpine orogen. Eclogae Geologicae Helvetiae, 97, 93-117.

Stüwe, K., 1997. Effective bulk composition changes due to cooling: a model predicting complexities in retrograde reaction textures. Contributions to Mineralogy and Petrology, 129, 43–52.

Tajcmanova, L., Connolly, J.A.D., Cesare, B., 2009. A thermodynamic model for titanium and ferric iron solution in biotite. Journal of Metamorphic Geology, 27, 153-165.

Ungaretti, L., Mazzi, F., Rossi, G., Dal Negro, A., 1981. Crystal-chemical characterization of blue amphiboles. Proc. XI Gen. Meeting I.M.A. Novosibirsk, Rock Forming Minerals, 82-110.

Wei, C., Powell, R., 2003. Phase relations in high-pressure metapelites in the system KFMASH (K_2O–FeO–MgO–Al_2O_3–SiO_2–H_2O) with application to natural rocks. Contributions to Mineralogy and Petrology, 145, 301-315.

Wei, C., Powell, R., 2004. Calculated phase relations in high-pressure metapelites in the system NKFMASH (Na_2O–K_2O–FeO–MgO–Al_2O_3– SiO_2–H_2O). Journal of Petrology, 45, 183-202.

White, R. W., Powell, R., Holland, T. J. B., 2007. Progress relating to calculation of partial melting equilibria for metapelites. Journal of Metamorphic Geology, 25, 511-527.

Zack, T., Rivers, T., Brumm, R. & Kronz, A., 2004. Cold subduction of oceanic crust: Implications from a lawsonite eclogite from the Dominican Republic. European Journal of Mineralogy, 16, 909–916.

FIGURE CAPTIONS

Fig. 1. a) Simplified tectonic map of Western Alps (modified after Schmid et al., 2004). b) Simplified geological map of the Gran Paradiso Massif (GP) and surrounding units (modified after Compagnoni and Lombardo, 1974). The location of the study area is indicated with a circle on the eastern margin of the GP.

Fig. 2. Simplified geological map of the study area showing the position of the studied samples. For a detailed geological map see Gasco et al. (2009).

Fig. 3. Field relationships between the studied rocks. a) Structural relationships between a well-preserved pre-S_1 eclogitic foliation and S_1 the regional foliation in metapelites; b) pre-S_1 foliation surface in metapelites defined by Wm + Qtz + Gln + Grt; c-d) fine-grained meta-aplites enveloping and crosscutting metagabbros. These structures are interpreted as preserving magmatic relationships suggesting that granitoids intruded the gabbros.

Fig. 4. Representative microstructures of the studied samples. a) re-equilibrated metapelite sample GMG17 with a well developed S_1 schistosity defined by Phe + Pg + Hbl + Zo + Ab + Grt + Qtz + Rt. Sample GMG2: b) eclogite facies foliation (pre-S_1) in metapelite defined by Qtz + Wm + Gln; c) pre-S_1 foliation cut by low-angle shear bands (regional foliation S_1) defined by white mica. d) sample GMG5: re-equilibrated metagabbro with a well developed S_1 regional foliation defined by Act + Zo + Pg + Phe + Chl + Ab + Rt. Sample GMG10: e) millimetre size OmpI crystal surrounded by OmpII + Grt aggregates and lozenge-shaped Pg + Zo + Qtz aggregates with later Act developing at the contact with the pseudomorphs and Omp; f) Pg + Zo + Qtz aggregates interpreted as pseudomorphs after Lws. Pg + Act show a preferred orientation related to the development of the S_1 foliation.

Fig. 5. Back-scattered images of the studied samples. Metagabbro GMG10: a) OmpI crystal surrounded by Grt and Ca-Am; b) detail of a Pg + Zo + Qtz aggregate with Zo and Pg including relics of OmpI suggesting destabilization of Lws via reaction Lws + Omp (Jd-rich) = Pg + Zo + Qtz; c) oriented Tlc + Qtz inclusions in an OmpI porphyroclast which is partially re-crystallized to OmpII (brighter patches on OmpI); d) small zoned garnet showing inclusions of Qtz. Metapelite GMG2: e) multistage garnet showing a rounded inclusion-rich core (GrtI) overgrown by idiomorphic GrtII around which a partial rim of GrtIII developed; f) matrix garnet showing a partially resorbed and fractured GrtII overgrown by idioblastic GrtIII; g) microfolded pre-eclogitic foliation defined by Pg + Phe; h) thin Hbl rim (AmII) around a Gln crystal (AmI) partially replaced by Qtz + Chl and by a symplectite of Bt + Chl (?).

Fig. 6. Mineral chemistry of metagabbro sample GMG10. a) zoning profile of a garnet grown in equilibrium with omphacite I. The rim at the right end of the profile shows a drop in Grs and Alm indicative of late re-equilibration and diffusion; b) composition of garnet grown in contact with omphacite and of garnet included in other minerals; c) composition of omphacite I and II; d)

composition of white mica: Phe shows a decreasing celadonite content from core to rim; e) composition of amphibole: glaucophane represents the HP stage while the amphibole defining the decompressional regional foliation is zoned from actinolite (core) to hornblende (rim); f) zoning profile (rim to core) of amphibole with glaucophane core and actinolite to hornblende rim.

Fig. 7. Mineral chemistry of sample GMG2. a) chemical core-rim profile of a multistage garnet showing three growth stages; b) zoning profile of a matrix garnet with the same composition as GrtII and GrtIII of a); c) Ca X-ray map of multistage garnet clearly showing the relationships between the three growth generations; d) composition of white mica: PheII shows decreasing celadonite content from core to rim; e) composition of amphibole: glaucophane represents the HP stage while hornblende defines the regional foliation; f) zoning profile of amphibole with a glaucophane core and an hornblende rim.

Fig. 8. a-d) P-T pseudosection for sample GMG10 calculated with SiO_2 saturated conditions for the unfractionated bulk composition reported in Table 4 (column A); b) contours intersection for three different composition (core, mantle, rim) of garnet. The position of the reaction for Jd + Lws = Zo + Pg + Qtz, calculated with PERPLE_X, and different geothermal gradients are also reported; c) contours for XMg and XJd in Omp showing that the omphacite with maximum XJd (0.50-0.52) is stable at the eclogitic peak; d) contours for Si a.p.f.u. in phengite and H_2O content (structurally bounded in minerals): H_2O decreases from 4 to 3 wt. % during garnet growth and to 1-2 wt. % during the following decompression in the Omp + Zo + Grt + Gln + Phe + Pg + Tlc + Qtz field. Exhumation is near-isothermal. e-f) PT pseudosection for sample GMG10 with SiO_2 saturated conditions after subtraction of the Grt core and the Grt core-mantle composition, respectively. The composition used are reported in Table 4 (columns B and C, respectively).

Fig. 9. a) P-T pseudosection for GrtI growth conditions of sample GMG2 for the XRF composition reported in Table 4 (column D); b) Alm, Grs and Prp mol. % contour intersection for GrtI core, mantle and rim using the unfractionated bulk rock composition; c-d) garnet mantle and rim contours after subtraction of the garnet core and of the core-mantle composition, respectively. The composition used are reported in Table 4 (columns E and F, respectively).

Fig. 10. a-b) P(T)-X pseudosection calculated to evaluate the effective bulk composition during GrtII growth in sample GMG2. The y-axis represents a 6 °C/km gradient. The left corner of the x-axis corresponds to the fractionation of GrtI from the initial composition reported in column G of Table 4 while the right end of the x-axis represent a bulk composition with 10 vol. % paragonite fractionated (column H in Table 4). In b) the contours for GrtII core composition intersect at 6.5 vol. % fractionated paragonite (see text for discussion); c-d) P-T pseudosection for GrtII growth conditions for the composition of column I of Table 4 derived from subtraction of 6.5 vol. % paragonite; d) contour intersection for core and rim composition of GrtII and Si a.p.f.u. isopleths for phengite. The PT path derived by the garnet growth zoning of GMG10 is reported in dark-grey; e) GrtII rim contour intersection after subtraction of the garnet core composition for the composition in column L (Table 4).

Fig. 11. a) PT pseudosection for GrtIII and M3 assemblage growing conditions for an effective rock composition reported in Table 4, column M; b) contour intersection for GrtIII composition; c) XMg contours for Hbl and Chl; d) vol. % of Grt. M3 equilibrated along an apparent geothermal gradient of 14-17 °C/km.

Fig. 12. Alpine PT path reconstructed for the eastern Gran Paradiso Massif according to the results obtained from metagabbro and metapelite. The PT paths of Brouwer et al. (2002) and of Le Bayon et

al. (2006) have been reported for comparison. The depth is calculated on the basis of an average density of 2.95 kg/dm^3 for subducted crust.

Table 1. Different metamorphic stages recognized for the two studied metagabbro and metapelite from the polymetamorphic Gneiss Minuti Complex at the eastern border of the Gran Paradiso Massif.

Table 2. Selected microprobe analyses for metagabbro GMG10 from the eastern border of the Gran Paradiso Massif.

Table 3. Selected microprobe analyses for metapelite GMG2 from the eastern border of the Gran Paradiso Massif.

Table 4. Chemical compositions used to calculate the pseudosections of Fig. 8-11.

FIGURES AND TABLES

FIG. 1

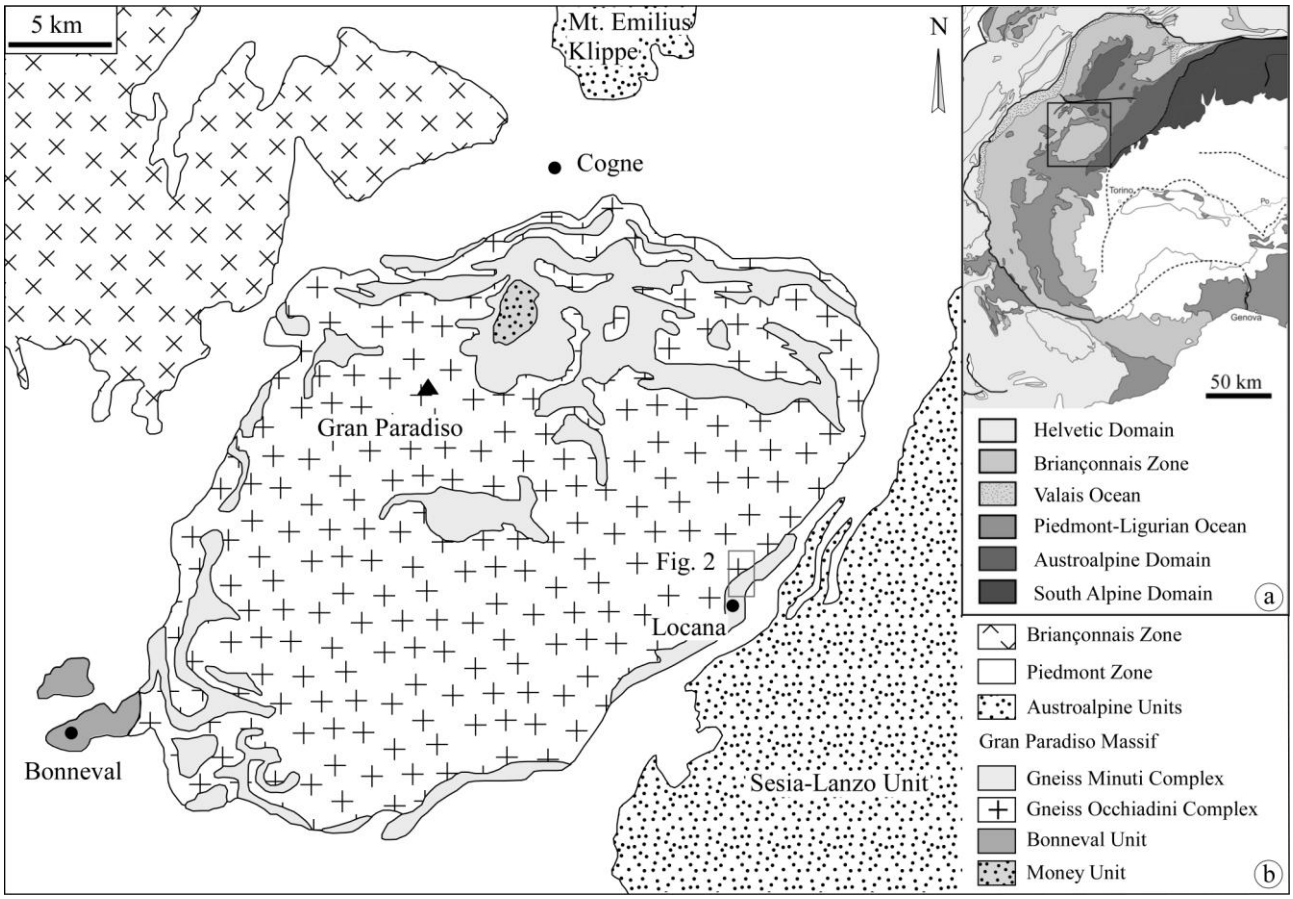

FIG. 2

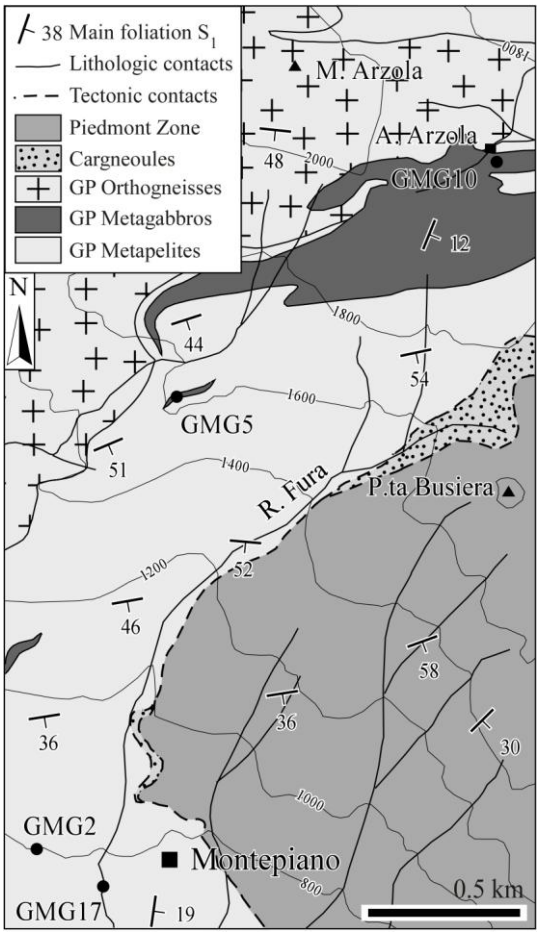
38 Main foliation S1
Lithologic contacts
Tectonic contacts
Piedmont Zone
Cargneoules
GP Orthogneisses
GP Metagabbros
GP Metapelites
M. Arzola
A. Arzola
GMG10
GMG5
GMG2
GMG17
Montepiano
R. Fura
P.ta Busiera
N
0.5 km
1800
2000
1600
1400
1200
1000
800
48
12
44
54
51
52
46
58
36
30
19

FIG. 3

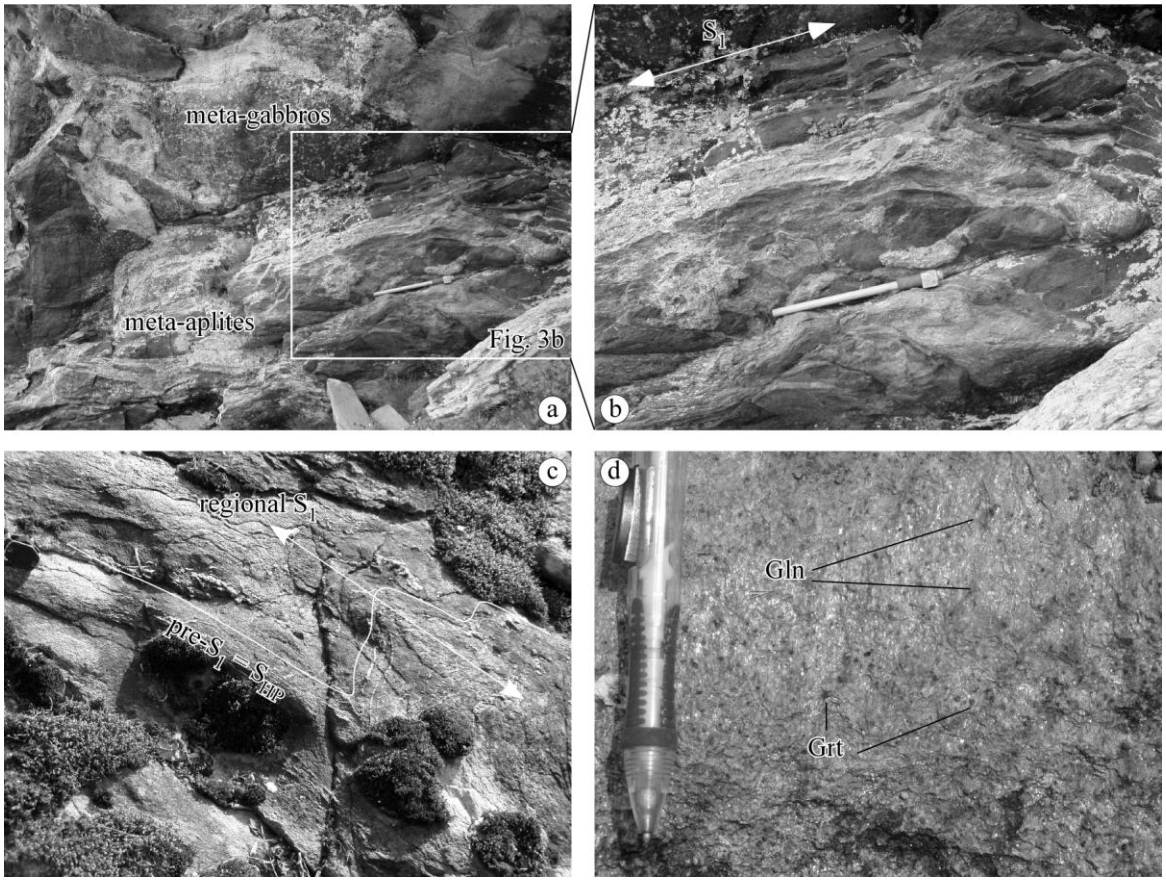
meta-gabbros
meta-aplites
Fig. 3b
a
S_1
b
c
regional S_1
pre-S_1 – S_{HP}
d
Gln
Grt

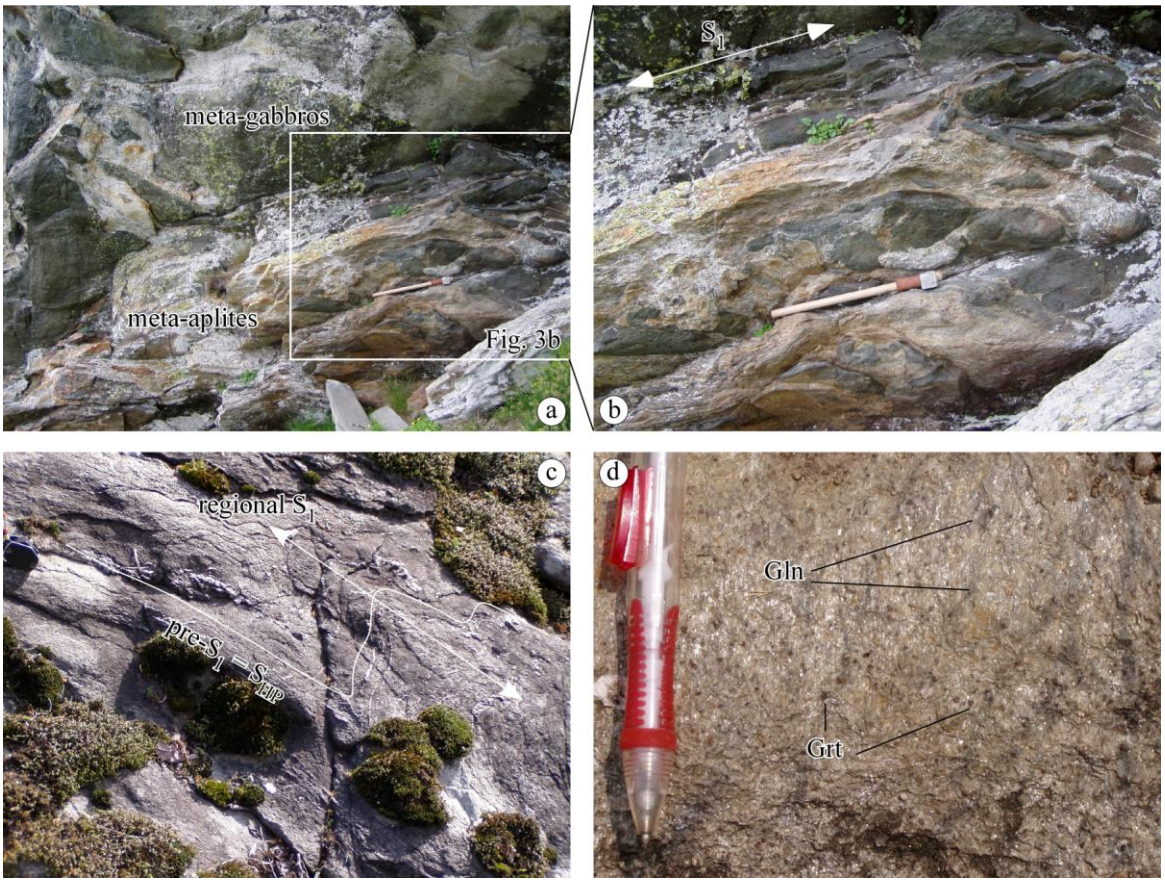
meta-gabbros
meta-aplites
Fig. 3b
a
S_1
b
c
regional S_1
pre-S_1 – S_{1P}
d
Gln
Grt

FIG. 4

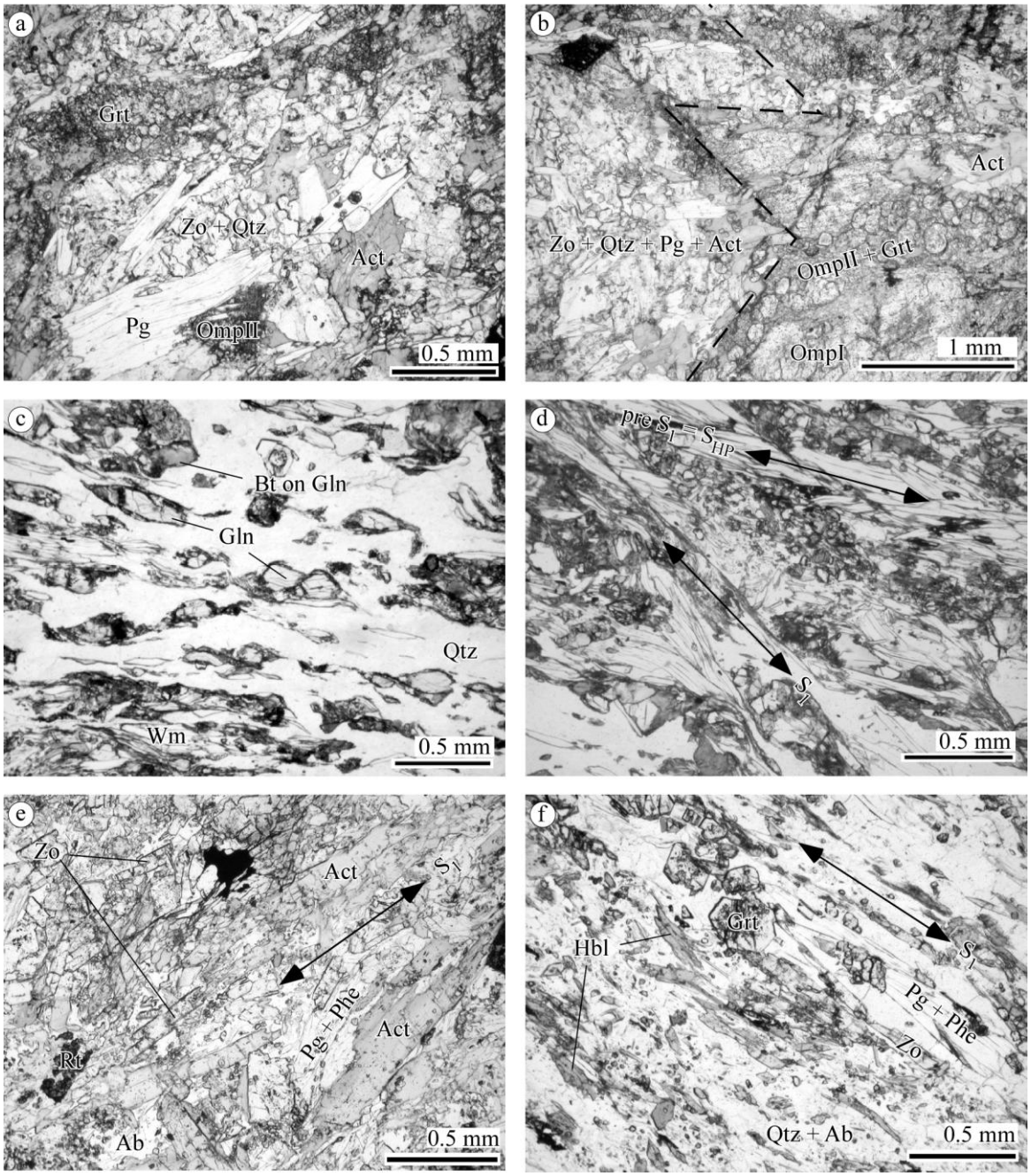
a
Grt
Zo + Qtz
Act
Pg
OmpII
0.5 mm
b
Act
Zo + Qtz + Pg + Act
OmpII + Grt
OmpI
1 mm
c
Bt on Gln
Gln
Qtz
Wm
0.5 mm
d
pre-S_1 = S_{HP}
S_1
0.5 mm
e
Zo
Act
S_1
Pg + Phe
Act
Rt
Ab
0.5 mm
f
Grt
Hbl
S_1
Pg + Phe
Zo
Qtz + Ab
0.5 mm

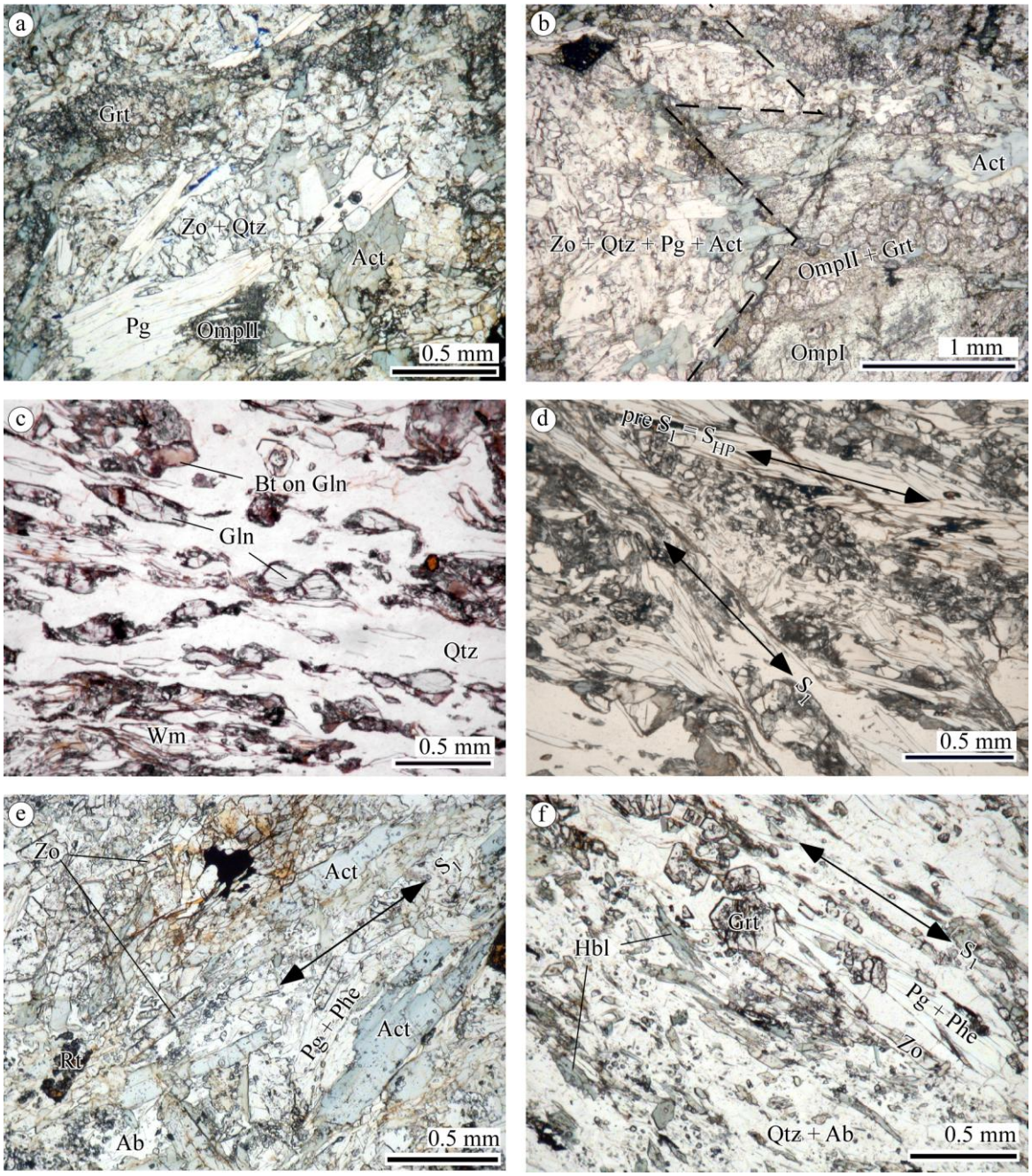
a
Grt
Zo + Qtz
Act
Pg
OmpII
0.5 mm
b
Act
Zo + Qtz + Pg + Act
OmpII + Grt
OmpI
1 mm
c
Bt on Gln
Gln
Qtz
Wm
0.5 mm
d
pre-S1 = SHP
S1
0.5 mm
e
Zo
Act
S1
Pg + Phe
Act
Rt
Ab
0.5 mm
f
Grt
Hbl
S1
Pg + Phe
Zo
Qtz + Ab
0.5 mm

FIG. 5

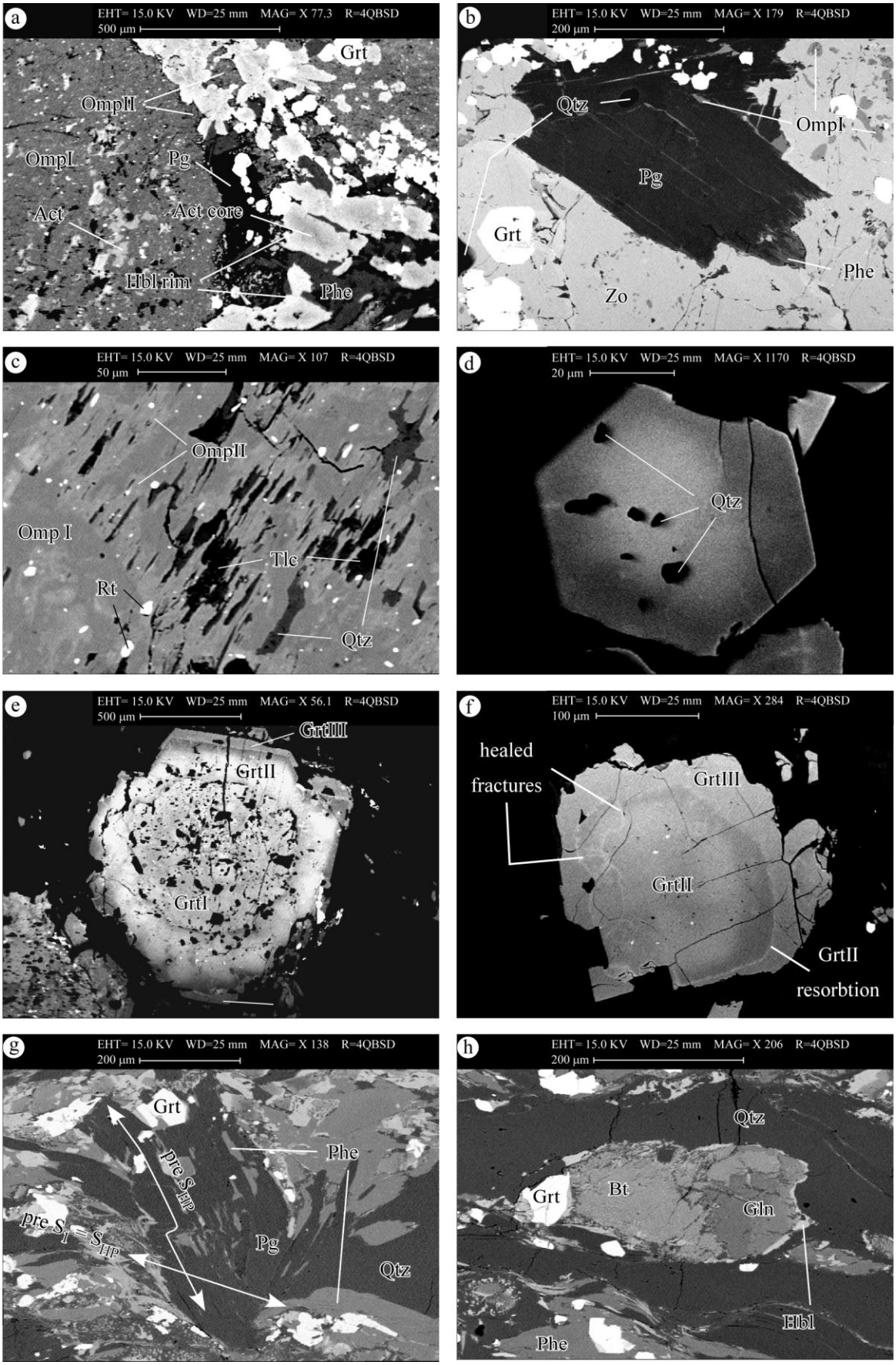
a
EHT= 15.0 KV WD=25 mm MAG= X 77.3 R=4QBSD
500 μm
Grt
OmpII
OmpI
Pg
Act
Act core
Ebl rim
Phe
b
EHT= 15.0 KV WD=25 mm MAG= X 179 R=4QBSD
200 μm
Qtz
OmpI
Pg
Grt
Phe
Zo
c
EHT= 15.0 KV WD=25 mm MAG= X 107 R=4QBSD
50 μm
OmpII
Omp I
Tlc
Rt
Qtz
d
EHT= 15.0 KV WD=25 mm MAG= X 1170 R=4QBSD
20 μm
Qtz
e
EHT= 15.0 KV WD=25 mm MAG= X 56.1 R=4QBSD
500 μm
GrtIII
GrtII
GrtI
f
EHT= 15.0 KV WD=25 mm MAG= X 284 R=4QBSD
100 μm
healed
fractures
GrtIII
GrtII
GrtII
resorbtion
g
EHT= 15.0 KV WD=25 mm MAG= X 138 R=4QBSD
200 μm
Grt
Phe
pre S_{HP}
pre $S_I = S_{HP}$
Pg
Qtz
h
EHT= 15.0 KV WD=25 mm MAG= X 206 R=4QBSD
200 μm
Qtz
Grt
Bt
Gln
Ebl
Phe

FIG. 6

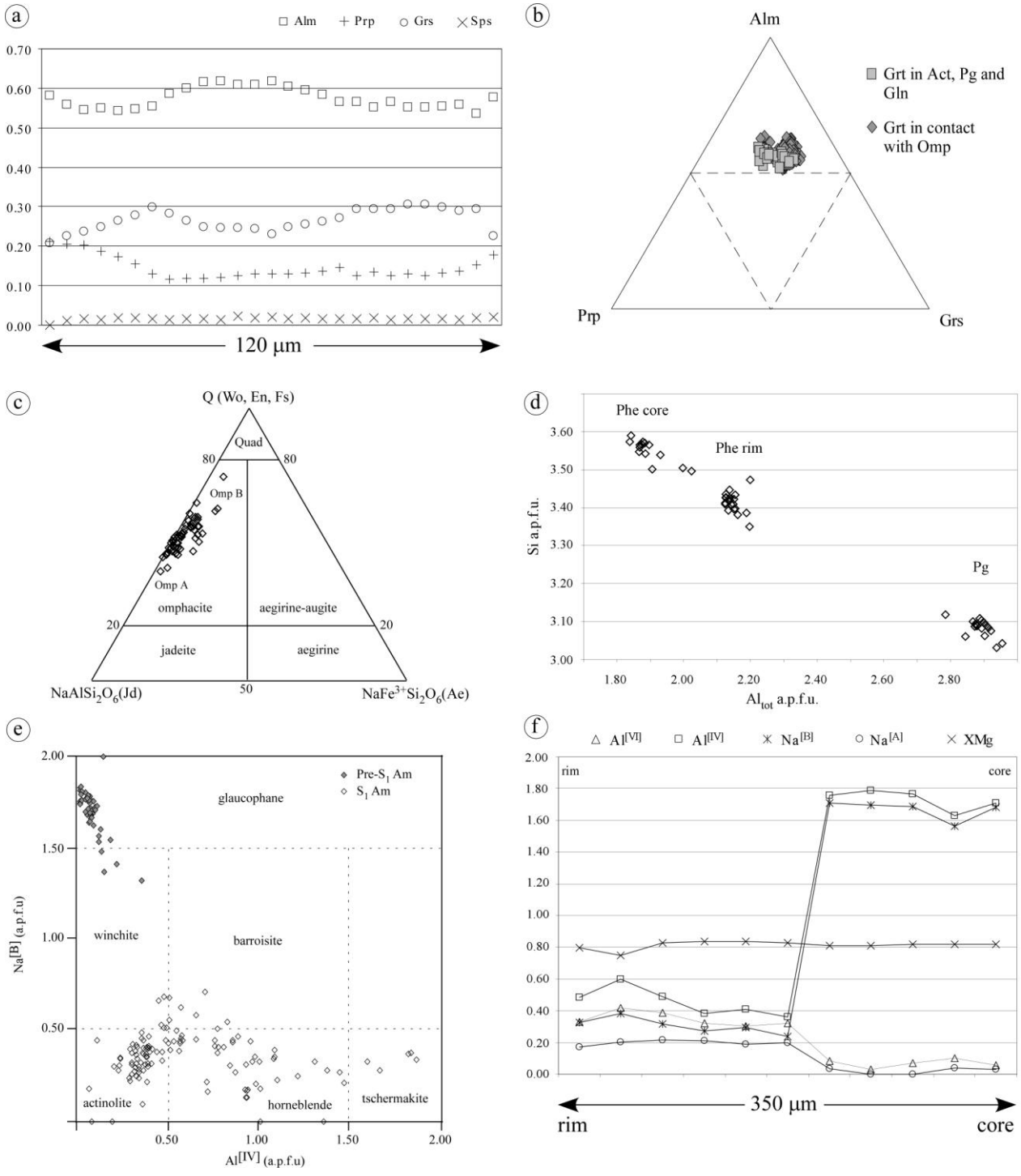
a
Alm
Prp
Grs
Sps
0.70
0.60
0.50
0.40
0.30
0.20
0.10
0.00
120 µm
b
Alm
Grt in Act, Pg and Gln
Grt in contact with Omp
Prp
Grs
c
Q (Wo, En, Fs)
Quad
80
80
Omp B
Omp A
omphacite
aegirine-augite
20
20
jadeite
aegirine
NaAlSi2O6(Jd)
50
NaFe3+Si2O6(Ae)
d
Phe core
Phe rim
Pg
Si a.p.f.u.
3.60
3.50
3.40
3.30
3.20
3.10
3.00
1.80
2.00
2.20
2.40
2.60
2.80
Altot a.p.f.u.
e
Pre-S1 Am
S1 Am
glaucophane
winchite
barroisite
actinolite
horneblende
tschermakite
Na[B] (a.p.f.u)
2.00
1.50
1.00
0.50
0.50
1.00
1.50
2.00
Al[IV] (a.p.f.u)
f
Al[VI]
Al[IV]
Na[B]
Na[A]
XMg
rim
core
2.00
1.80
1.60
1.40
1.20
1.00
0.80
0.60
0.40
0.20
0.00
350 µm
rim
core

FIG. 7

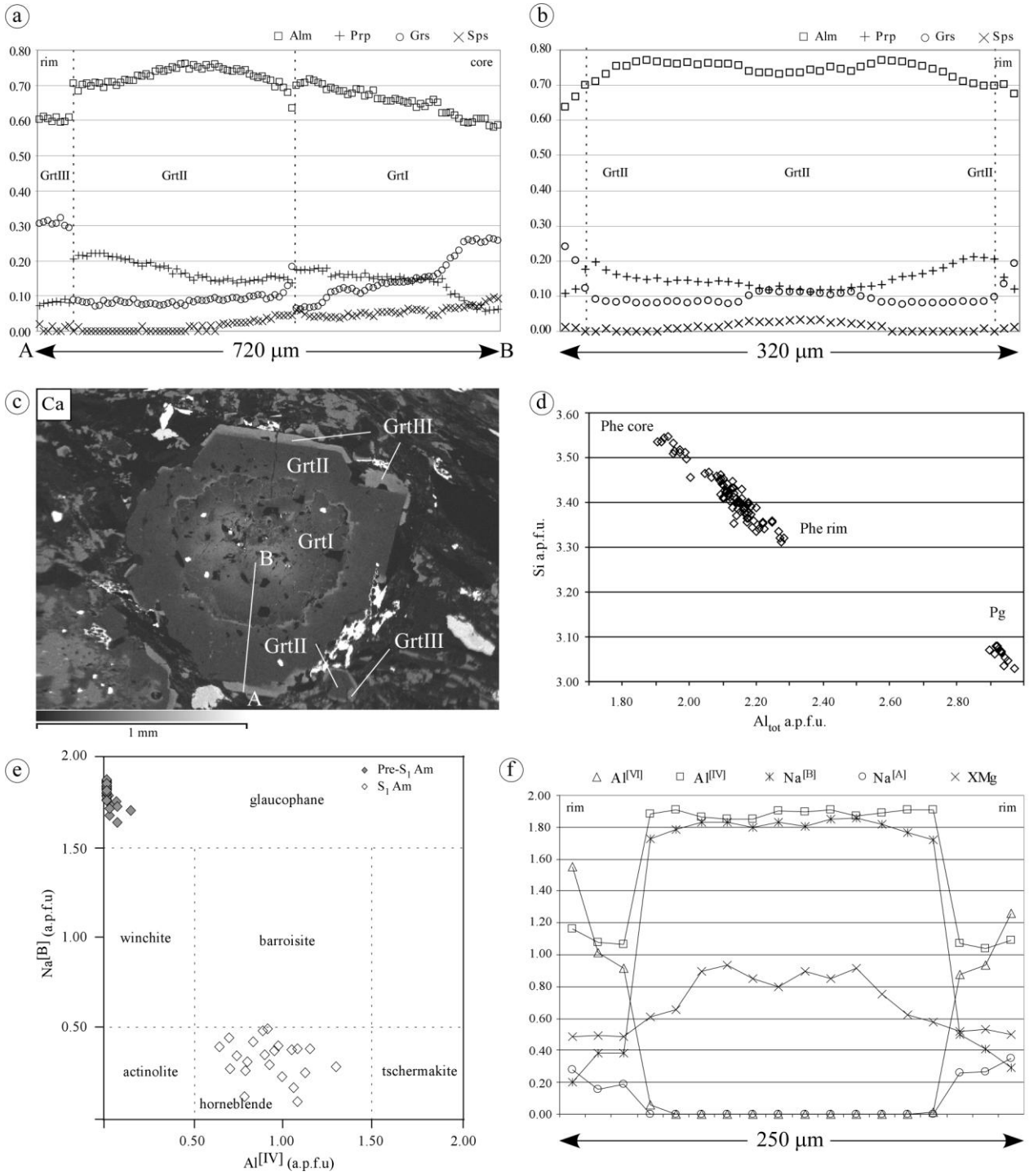
a
Alm
Prp
Grs
Sps
rim
core
GrtIII
GrtII
GrtI
A
720 µm
B
b
rim
GrtII
320 µm
c
Ca
GrtIII
GrtII
GrtI
B
A
1 mm
d
Phe core
Phe rim
Pg
Si a.p.f.u.
Al tot a.p.f.u.
e
Pre-S1 Am
S1 Am
glaucophane
winchite
barroisite
actinolite
tschermakite
horneblende
Na[B] (a.p.f.u)
Al[IV] (a.p.f.u)
f
Al[VI]
Al[IV]
Na[B]
Na[A]
XMg
rim
250 µm

FIG. 8

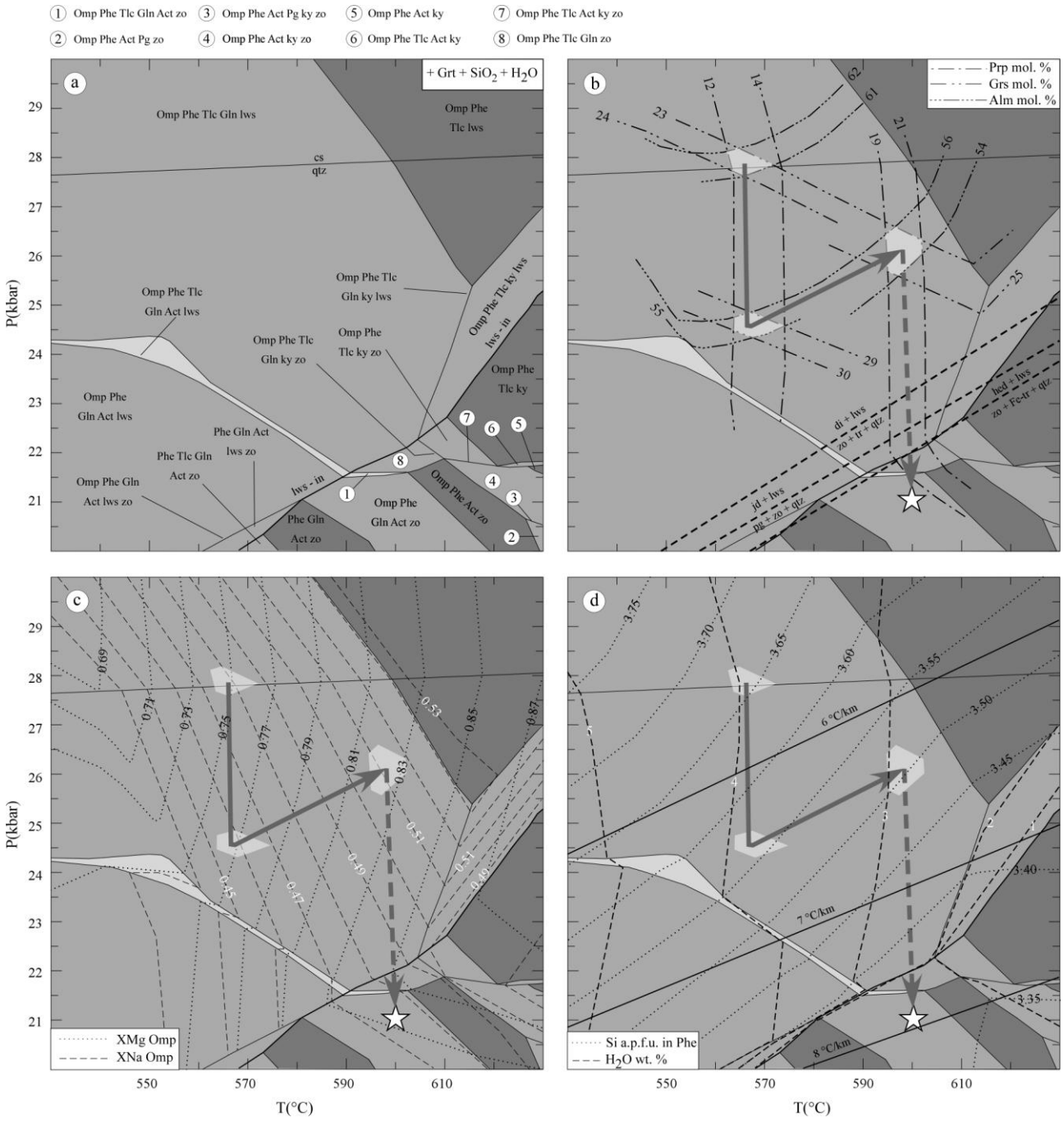
1 Omp Phe Tlc Gln Act zo
2 Omp Phe Act Pg zo
3 Omp Phe Act Pg ky zo
4 Omp Phe Act ky zo
5 Omp Phe Act ky
6 Omp Phe Tlc Act ky
7 Omp Phe Tlc Act ky zo
8 Omp Phe Tlc Gln zo
a
+ Grt + SiO2 + H2O
Omp Phe Tlc Gln lws
Omp Phe Tlc lws
cs
qtz
Omp Phe Tlc Gln Act lws
Omp Phe Tlc Gln ky lws
Omp Phe Tlc ky lws - in
Omp Phe Tlc Gln ky zo
Omp Phe Tlc ky zo
Omp Phe Tlc ky
Omp Phe Gln Act lws
Phe Gln Act lws zo
Phe Tlc Gln Act zo
Omp Phe Gln Act lws zo
lws - in
Omp Phe Act zo
Omp Phe Gln Act zo
Phe Gln Act zo
b
Prp mol. %
Grs mol. %
Alm mol. %
hed + lws
zo + Fe-tr + qtz
di + lws
zo + tr + qtz
jd + lws
grt + zo + qtz
c
XMg Omp
XNa Omp
d
Si a.p.f.u. in Phe
H2O wt. %
6 °C/km
7 °C/km
8 °C/km
P(kbar)
T(°C)

FIG. 9

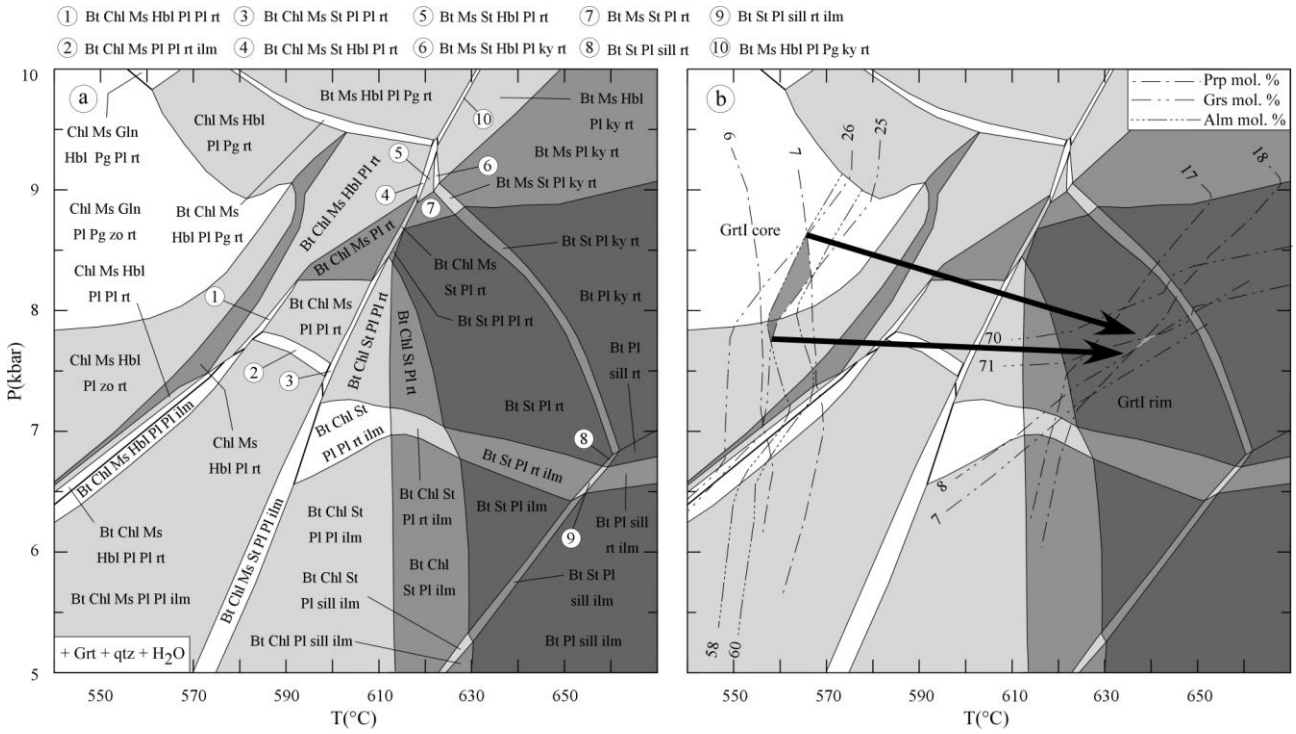
① Bt Chl Ms Hbl Pl Pl rt
② Bt Chl Ms Pl Pl rt ilm
③ Bt Chl Ms St Pl Pl rt
④ Bt Chl Ms St Hbl Pl rt
⑤ Bt Ms St Hbl Pl rt
⑥ Bt Ms St Hbl Pl ky rt
⑦ Bt Ms St Pl rt
⑧ Bt St Pl sill rt
⑨ Bt St Pl sill rt ilm
⑩ Bt Ms Hbl Pl Pg ky rt
a
b
P(kbar)
T(°C)
+ Grt + qtz + H2O
Prp mol. %
Grs mol. %
Alm mol. %
GrtI core
GrtI rim

FIG. 10

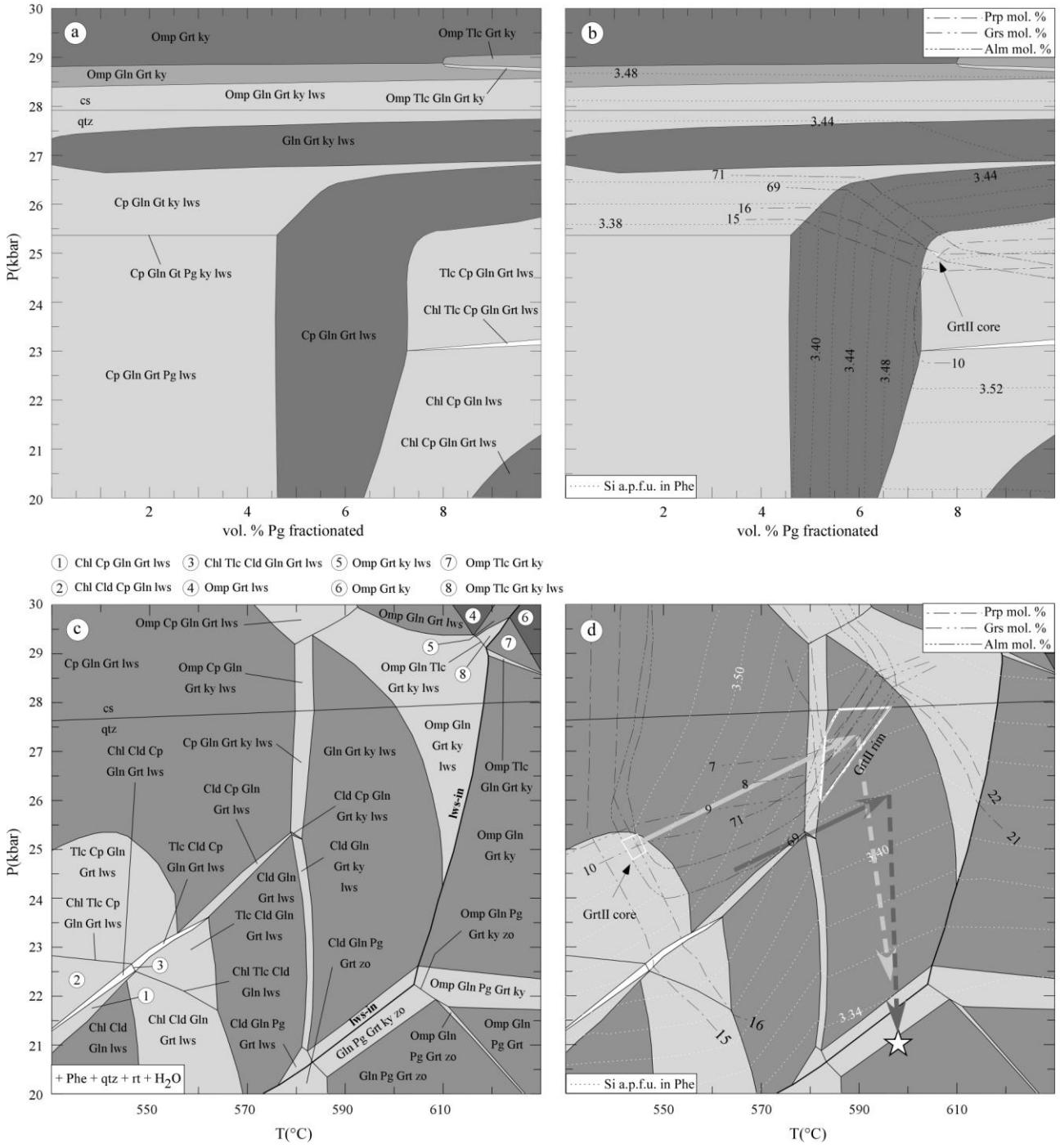
a
Omp Grt ky
Omp Tlc Grt ky
Omp Gln Grt ky
cs
Omp Gln Grt ky lws
Omp Tlc Gln Grt ky
qtz
Gln Grt ky lws
Cp Gln Gt ky lws
Cp Gln Gt Pg ky lws
Tlc Cp Gln Grt lws
Chl Tlc Cp Gln Grt lws
Cp Gln Grt lws
Cp Gln Grt Pg lws
Chl Cp Gln lws
Chl Cp Gln Grt lws
P(kbar)
vol. % Pg fractionated
b
Prp mol. %
Grs mol. %
Alm mol. %
3.48
3.44
71
69
16
15
3.38
3.44
GrtII core
10
3.40
3.44
3.48
3.52
Si a.p.f.u. in Phe
vol. % Pg fractionated
1 Chl Cp Gln Grt lws
2 Chl Cld Cp Gln lws
3 Chl Tlc Cld Gln Grt lws
4 Omp Grt lws
5 Omp Grt ky lws
6 Omp Grt ky
7 Omp Tlc Grt ky
8 Omp Tlc Grt ky lws
c
Omp Cp Gln Grt lws
Omp Gln Grt lws
Cp Gln Grt lws
Omp Cp Gln Grt ky lws
Omp Gln Tlc Grt ky lws
cs
qtz
Omp Gln Grt ky lws
Chl Cld Cp Gln Grt lws
Cp Gln Grt ky lws
Gln Grt ky lws
Cld Cp Gln Grt lws
Cld Cp Gln Grt ky lws
lws-in
Omp Tlc Gln Grt ky
Tlc Cp Gln Grt lws
Tlc Cld Cp Gln Grt lws
Cld Gln Grt ky lws
Omp Gln Grt ky
Chl Tlc Cp Gln Grt lws
Cld Gln Grt lws
Tlc Cld Gln Grt lws
Omp Gln Pg Grt ky zo
Cld Gln Pg Grt zo
Chl Tlc Cld Gln lws
Omp Gln Pg Grt ky
Chl Cld Gln lws
Chl Cld Gln Grt lws
Cld Gln Pg Grt lws
lws-in
Gln Pg Grt ky zo
Omp Gln Pg Grt zo
Omp Gln Pg Grt
Gln Pg Grt zo
+ Phe + qtz + rt + H_2O
P(kbar)
T(°C)
d
Prp mol. %
Grs mol. %
Alm mol. %
3.50
7
8
9
71
69
GrtII rim
25
21
3.40
10
GrtII core
16
15
3.34
Si a.p.f.u. in Phe
T(°C)

FIG. 11

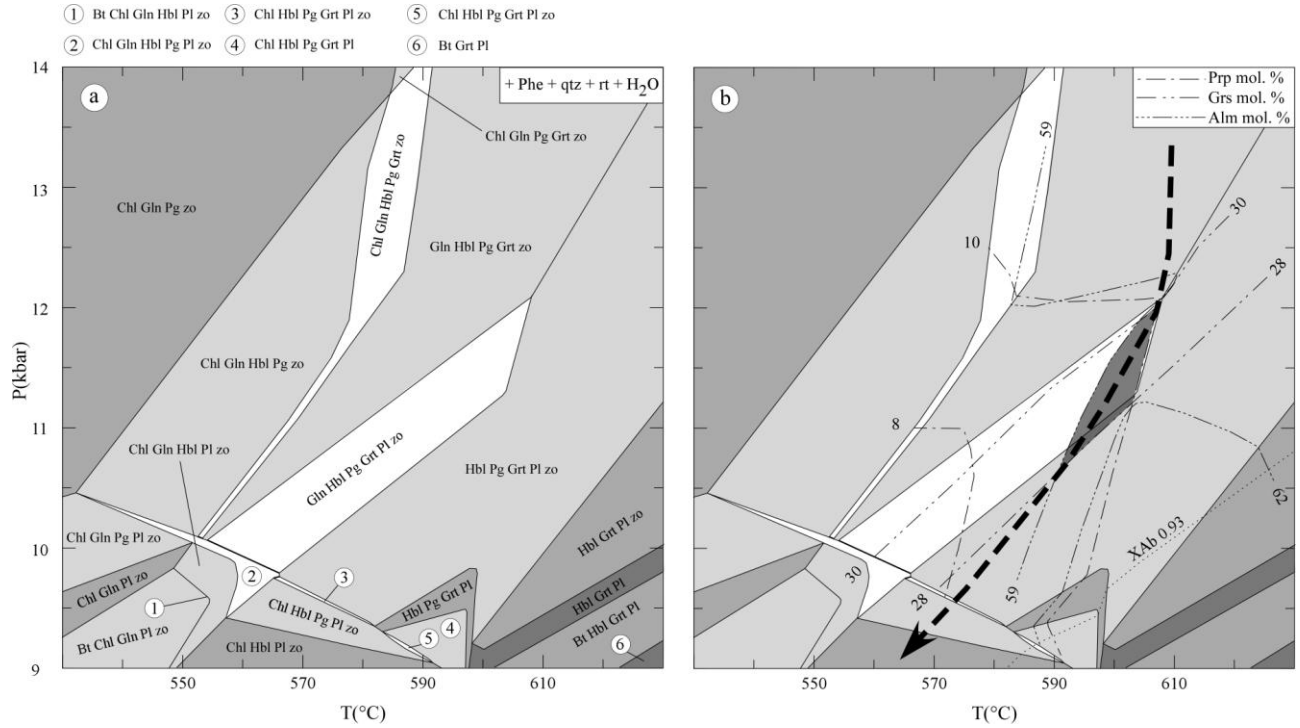
1 Bt Chl Gln Hbl Pl zo
2 Chl Gln Hbl Pg Pl zo
3 Chl Hbl Pg Grt Pl zo
4 Chl Hbl Pg Grt Pl
5 Chl Hbl Pg Grt Pl zo
6 Bt Grt Pl
a
+ Phe + qtz + rt + H2O
Chl Gln Pg Grt zo
Chl Gln Hbl Pg Grt zo
Chl Gln Pg zo
Gln Hbl Pg Grt zo
Chl Gln Hbl Pg zo
Chl Gln Hbl Pl zo
Gln Hbl Pg Grt Pl zo
Hbl Pg Grt Pl zo
Chl Gln Pg Pl zo
Hbl Grt Pl zo
Chl Gln Pl zo
Hbl Pg Grt Pl
Hbl Grt Pl
Chl Hbl Pg Pl zo
Bt Chl Gln Pl zo
Chl Hbl Pl zo
Bt Hbl Grt Pl
P(kbar)
T(°C)
b
Prp mol. %
Grs mol. %
Alm mol. %
XAb 0.93

FIG. 12

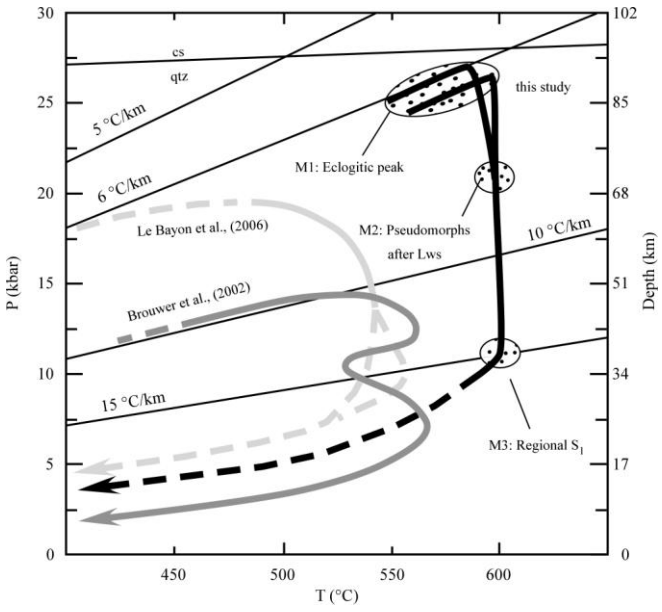
cs
qtz
5 °C/km
6 °C/km
10 °C/km
15 °C/km
this study
M1: Eclogitic peak
M2: Pseudomorphs after Lws
M3: Regional S1
Le Bayon et al., (2006)
Brouwer et al., (2002)
P (kbar)
Depth (km)
T (°C)

TAB. 1

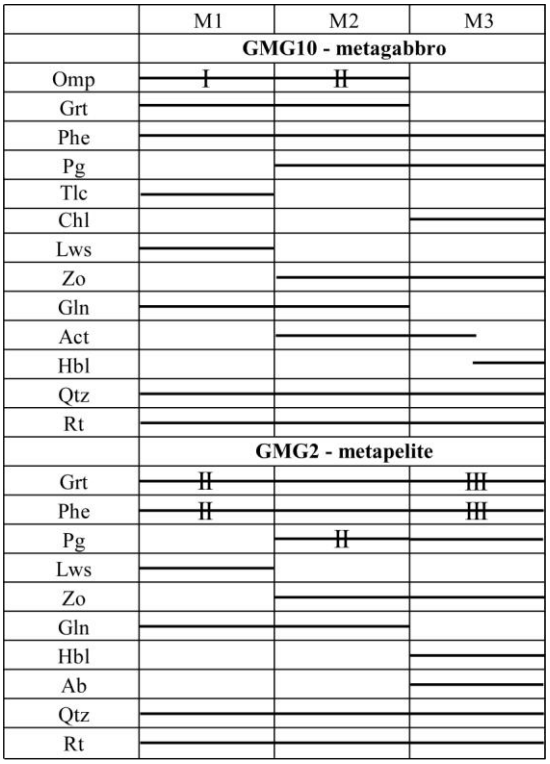

TAB. 2

GMG10	**Omp**		**Grt***		**Wm**			**Am***		**Tlc**	**Zo**
Analysis	s1px2	s1px7	grt16	grt1	s4phe4	wm10	s2pa8	amph11c	amph1r	tlc2	zo2
Position	core	rim	core	rim	core	rim		core	rim		
	OmpI	OmpII			Phe	Phe	Pg	Gln	Act		
SiO_2	57.44	56.76	38.57	39.22	54.50	50.73	48.18	58.59	54.86	61.17	40.38
TiO_2	0.00	0.00	0.00	0.00	0.38	0.00	0.00	0.00	0.00	0.00	0.00
Cr_2O_3	0.66	0.44	0.00	0.00	0.00	0.00	0.00	0.00	0.00	0.00	0.00
Al_2O_3	12.10	9.32	21.06	21.35	23.73	27.83	38.05	11.96	4.94	0.00	31.40
FeO_{tot}	2.44	2.01	28.33	27.43	1.44	1.87	0.68	6.14	7.97	6.01	1.53
MnO	0.00	0.00	0.75	0.68	0.00	0.00	0.00	0.00	0.00	0.00	0.00
MgO	8.26	9.84	3.41	5.83	4.78	3.22	0.00	12.19	17.41	27.78	0.00
NiO	0.00	0.00	0.00	0.00	0.00	0.00	0.00	0.00	0.00	0.00	0.00
CaO	11.78	14.92	9.10	6.82	0.00	0.00	0.00	1.31	10.89	0.00	25.01
Na_2O	7.58	6.07	0.00	0.00	0.00	0.91	7.11	6.78	1.82	0.00	0.00
K_2O	0.00	0.00	0.00	0.00	11.30	10.65	1.10	0.00	0.00	0.00	0.00
Sum	100.26	99.36	101.22	101.33	96.13	95.21	95.12	96.98	97.89	94.95	98.32
Fe_2O_3	0.00	0.58	0.00	0.00	0.00	0.26	0.00	0.00	0.00	0.00	1.38
Si	2.011	2.013	3.014	3.023	3.590	3.349	3.087	7.945	7.670	3.990	3.066
Ti	0.000	0.000	0.000	0.000	0.009	0.000	0.000	0.000	0.000	0.000	0.000
Cr	0.018	0.012	0.000	0.000	0.000	0.000	0.000	0.000	0.000	0.000	0.000
Al	0.499	0.390	1.940	1.940	1.842	2.198	2.874	1.911	0.815	0.000	2.810
Fe^{3+}	0.000	0.016	0.000	0.000	0.000	0.126	0.000	0.000	0.000	0.330	0.079
Fe^{2+}	0.071	0.060	1.852	1.768	0.079	0.000	0.036	0.697	0.932	0.000	0.000
Mn	0.000	0.000	0.050	0.044	0.000	0.001	0.000	0.000	0.000	0.000	0.000
Mg	0.431	0.520	0.397	0.670	0.469	0.327	0.000	2.464	3.628	2.700	0.000
Ni	0.000	0.000	0.000	0.000	0.000	0.000	0.000	0.000	0.000	0.000	0.000
Ca	0.442	0.567	0.762	0.563	0.000	0.000	0.000	0.191	1.631	0.000	2.035
Na	0.515	0.417	0.000	0.000	0.000	0.082	0.883	1.783	0.494	0.000	0.000
K	0.000	0.000	0.000	0.000	0.949	0.865	0.090	0.000	0.000	0.000	0.000
Sum	3.987	3.995	8.015	8.008	6.938	6.947	6.971	14.991	15.170	7.020	7.990

Fe_2O_3 and Fe^{3}+ calculated according to Ulmer (1993); *assuming all ferrous iron

TAB. 3

GMG2	**GrtI***		**GrtII***		**GrtIII***	**Wm**			**Am***		**Zo**
Analysis	grt111	grt63	grt60	grt10	grt2	wm20c	wm16r	wm2	anf47c	anf39r	zo2
Position	core	rim	core	rim		core	rim		core	rim	
						PheII	PheIII	Pg	Gln	Hbl	
SiO_2	38.01	37.42	37.96	37.18	37.78	53.76	51.90	48.47	60.82	47.62	39.71
TiO_2	0.00	0.00	0.00	0.00	0.00	0.00	0.00	0.00	0.00	0.00	0.00
Cr_2O_3	0.00	0.00	0.00	0.00	0.00	0.00	0.00	0.00	0.00	0.00	0.00
Al_2O_3	20.67	20.68	20.56	20.93	20.96	25.20	26.89	39.31	12.21	12.08	28.01
FeO_{tot}	26.19	32.10	30.62	31.78	27.56	1.32	1.91	0.00	6.07	18.33	6.91
MnO	4.29	2.62	2.06	0.59	0.01	0.00	0.00	0.00	0.00	0.00	0.00
MgO	1.56	4.40	3.72	5.63	2.04	4.65	3.73	0.00	11.97	9.92	0.00
NiO	0.00	0.00	0.00	0.00	0.00	0.00	0.00	0.00	0.00	0.00	0.00
CaO	9.26	2.22	4.51	3.17	11.16	0.00	0.00	0.00	7.079	7.10	24.57
Na_2O	0.00	0.00	0.00	0.00	0.00	0.00	0.53	7.44	0.00	1.91	0.00
K_2O	0.00	0.00	0.00	0.00	0.00	11.16	10.59	0.48	0.00	0.85	0.00
Sum	99.98	99.44	99.43	99.28	99.51	96.09	95.55	95.70	98.15	97.80	99.20
Fe_2O_3	0.00	0.00	0.00	0.00	0.00	0.99	1.18	0.00	0.00	0.00	6.22
Si	3.007	3.001	3.037	2.953	3.005	3.532	3.439	3.067	8.000	6.989	3.044
Ti	0.001	0.001	0.001	0.001	0.001	0.000	0.000	0.000	0.000	0.000	0.000
Cr	0.000	0.000	0.000	0.000	0.000	0.000	0.000	0.000	0.000	0.000	0.000
Al	1.916	1.954	1.940	1.959	1.966	1.951	2.100	2.931	1.893	2.090	2.531
Fe^{3+}	0.000	0.000	0.000	0.000	0.000	0.049	0.059	0.000	0.486	0.000	0.400
Fe^{2+}	1.812	2.154	2.050	2.126	1.837	0.002	0.033	0.000	0.274	0.000	0.000
Mn	0.286	0.178	0.140	0.040	0.001	0.000	0.000	0.000	0.000	2.249	0.000
Mg	0.193	0.526	0.444	0.667	0.242	0.455	0.369	0.000	2.347	2.170	0.000
Ni	0.000	0.000	0.000	0.000	0.000	0.000	0.000	0.000	0.000	0.000	0.000
Ca	0.793	0.191	0.387	0.270	0.952	0.000	0.000	0.000	0.191	1.12	2.018
Na	0.000	0.000	0.000	0.000	0.000	0.000	0.068	0.913	1.805	0.54	0.000
K	0.000	0.000	0.000	0.000	0.000	0.935	0.895	0.039	0.000	0.16	0.000
Sum	8.008	8.005	7.998	8.015	8.003	6.925	6.963	6.949	14.996	15.318	7.993

Fe_2O_3 and Fe^3+ calculated according to Ulmer (1993); *assuming all ferrous iron

TAB. 4

	GMG10	**GMG2**			
	Fig. 8	Fig. 9	Fig. 10 a, b	Fig. 10 c, d	Fig. 11
	XRF	*XRF*	*- GrtI*	*-GrtI and PgI*	*- GrtI and Gln*
SiO_2	49.99	60.08	61.18	62.08	64.50
Al_2O_3	17.82	19.42	19.36	17.55	18.87
FeO	8.51	7.84	6.69	7.23	4.74
CaO	10.10	2.27	2.16	2.34	2.73
MgO	8.26	3.79	3.79	4.11	2.01
Na_2O	3.14	3.16	3.32	2.96	2.10
K_2O	0.55	2.38	2.50	2.65	3.60
TiO_2	1.46	0.94	0.99	1.07	1.45
MnO	0.17	0.12	0.01	0.01	0.001
Sum	100.00	100.00	100.00	100.00	100.00